Identifying four obesity axes through integrative multi-omics and imaging analysis

Odoemelam, C.S., Naz, A., Thanaj, M., Sorokin, E., Whitcher, B., Sattar, N., Bell, J.D., Thomas, E.L., Cule, M. and Yaghootkar, H.

Identifying four obesity axes through integrative multi-omics and imaging analysis

Running title: Obesity Axes: MRI Insights and Disease Links

Chiemela S. Odoemelam[1]*(me@chiemelao.com), Afreen Naz[1]*(ANaz@lincoln.ac.uk), Marjola Thanaj[2] (M.Thanaj@westminster.ac.uk), Elena P Sorokin[3] (sorokin@calicolabs.com), Brandon Whitcher[2] (B.Whitcher@westminster.ac.uk), Naveed Sattar[4] (Naveed.Sattar@glasgow.ac.uk), Jimmy D Bell[2] (J.Bell@westminster.ac.uk), E Louise Thomas[2] (l.thomas3@westminster.ac.uk), Madeleine Cule[3](cule@calicolabs.com), Hanieh Yaghootkar[1‡](HYaghootkar@lincoln.ac.uk)

[1]School of Natural Science, College of Health and Science, University of Lincoln, Lincoln, UK

[2]Research Center for Optimal Health, School of Life Sciences, University of Westminster, London, UK

[3]Calico Life Sciences LLC, South San Francisco, CA

[4]School of Cardiovascular and Metabolic Health, University of Glasgow, Glasgow, UK

* Contributed equally

‡Corresponding authors:

Hanieh Yaghootkar: HYaghootkar@lincoln.ac.uk (+44 7576890854)

Keywords: Obesity Subtypes, Magnetic Resonance Imaging, Precision Medicine, Ectopic Fat, Mendelian Randomization, Genome-Wide Association Studies, Body Composition Analysis

Word count: 4500; #Figures: 6; #Tables: 1

Abstract

We aimed to identify distinct axes of obesity using advanced MRI-derived phenotypes.

We used 24 MRI-derived fat distribution and muscle volume measures (UK Biobank, n= 33,122) to construct obesity axes through principal component analysis (PCA). Genome-wide association studies were performed for each axis to uncover genetic factors, followed by pathway enrichment, genetic correlation, and Mendelian randomization analyses to investigate disease associations.

Four primary obesity axes were identified: (1) General Obesity, reflecting higher fat accumulation in all regions (visceral, subcutaneous, and ectopic fat); (2) Muscle-Dominant, indicating greater muscle volume; (3) Peripheral Fat, associated with higher subcutaneous fat in abdominal and thigh regions; and (4) Lower Body Fat, characterized by increased lower-body subcutaneous fat and reduced ectopic fat. Each axis was associated with distinct genetic loci and pathways. For instance, the Lower Body Fat Axis was associated with *RSPO3* and *COBLL1* which are emerging as promising candidates for therapeutic targeting. Disease risks varied across axes: the General Obesity Axis correlated with higher risks of metabolic and cardiovascular diseases; the Lower Body Fat Axis appeared protective against type 2 diabetes and cardiovascular disease.

This study highlights the heterogeneity of obesity through the identification of obesity axes and emphasizes the potential to extend beyond BMI in defining and treating obesity for obesity-related disease management.

Article Highlights

- This study aimed to address potential limitations of BMI by exploring the heterogeneity of obesity using MRI-derived fat distribution and muscle volume measures.
- We sought to identify distinct obesity axes and investigate their genetic, metabolic, and disease associations.
- Four obesity axes were identified: General Obesity, Muscle-Dominant, Peripheral Fat, and Lower Body Fat, each linked to unique genetic loci, metabolic traits, and disease risks.
- These findings emphasize the potential to extend beyond BMI in defining and managing obesity, offering a more nuanced framework for understanding and treating obesity-related diseases.

Introduction

Obesity presents with a range of metabolic patterns, disease risks, and responses to weight loss interventions among individuals.(1-4) This variability is largely due to the traditional clinical definition of obesity, which uses a BMI threshold of over 30 to identify at-risk groups.(1) While this measure effectively categorises obesity at the population level, it fails to capture the heterogeneity among individuals.(5) This broad metric, while useful for public health strategies, is inadequate for the nuanced requirements of precision medicine that necessitate tailored approaches.

Numerous studies have explored the complexities of obesity by identifying specific subtypes, notably focusing on "metabolically healthy obesity," where individuals exhibit no initial metabolic dysfunctions despite living with obesity.(6) However, the stability of this state is uncertain, as many may develop metabolic complications over time as they gain weight or age.(2, 6) The use of biomarkers to classify obesity into subtypes and guide personalized treatments has been proposed.(2, 7) Yet, gathering biomarker data post-diagnosis can challenge causal interpretations due to potential reverse causation, where the disease itself might influence biomarker levels.(8) Additionally, the reliance on BMI hinders these methods as it fails to differentiate between fat and muscle mass or consider the importance of fat distribution.(1, 2) These limitations mean that even those within a normal BMI range can face metabolic challenges, whereas some individuals with obesity might display metabolic resilience.(2, 9)

Recent advancements in magnetic resonance imaging (MRI) technology and the availability of comprehensive scan data from participants in the UK Biobank have opened new avenues for detailed assessments of fat and muscle across various body regions. These image-derived phenotypes (IDPs) enable the classification of obesity axes without preconceived hypotheses by examining diverse fat distribution patterns in subcutaneous and ectopic locations.

In this study, we used 24 MRI-derived fat distribution and muscle measurements to agnostically construct four principal component (PC)-derived obesity axes. These axes are linear combinations of the IDPs, representing distinct dimensions of obesity, and allow us to move beyond traditional BMI classifications. We demonstrate that these axes capture unique patterns of fat distribution and muscle volume that are linked to different genetic profiles and disease risks. By integrating advanced imaging with genetic analysis, this study offers a comprehensive framework to better understand obesity heterogeneity, paving the way potentially for more targeted approaches in obesity management and treatment.

Methods

Study design

We applied 24 MRI-derived measures of fat distribution (volumes and percentages) and muscle indices from the UK Biobank to construct obesity axes. Analyses were conducted separately for males and females due to known sex-specific differences in fat distribution patterns. After confirming consistent principal component (PC) patterns across sexes, we performed meta-analyses of genome-wide association studies (GWAS) results for each axis. We investigated genetic correlations with metabolic biomarkers, lifestyle, behaviour, and psychological disorders. Additionally, we performed Mendelian randomization to explore relationships between each axis and obesity-related disease risks.

Image-derived measures of fat distribution and muscle volume

We employed neck-to-knee Dixon MRI and single-slice multi-echo MRI acquisitions for abdominal imaging, as previously outlined in the UK Biobank protocol.(10) Image processing was conducted using deep learning models as previously described.(11-14) The image-derived phenotypes (IDPs) included volume and median proton density fat fraction (PDFF), calculated via the Phase Regularized Estimation using the Smoothing and Constrained Optimization (PRESCO) method.(15) Quality control was performed by analyzing univariate distributions and visually inspecting scans for anomalies.

Supplementary table 1 details the 24 IDPs used in this study, including subcutaneous adipose tissue (SAT) volumes (abdominal and thigh), visceral adipose tissue (VAT) volumes, internal fat and thigh intermuscular adipose tissue volumes (corrected for muscle volume), iliopsoas and total muscle volumes (indexed to height^2). We also obtained a measure of fat (PDFF) stored in the liver, pancreas, and paraspinal muscles (intramyocellular fat) from the single-slice multi-echo acquisition.

Construction of obesity axes

Principal component analysis (PCA) was applied to the 24 IDPs to identify obesity axes. PCA, a robust and widely validated dimensionality reduction technique, captures dominant patterns of variation across datasets while minimizing noise. Each IDP was scaled and standardized to mean zero and unit variance. Resultant PCs were oriented to align with higher obesity levels. The number of PCs retained was determined based on the proportion of variance explained (>85% cumulatively), and the interpretability of the components.

Given sex-specific differences in fat and muscle distribution, PCA was conducted separately for males and females. Meta-analysis was subsequently performed on follow-up analyses (e.g. GWAS) for consistent axes across sexes, ensuring that male PC1 aligned with female PC1, male PC2 with female PC2, and so forth.

We did not include BMI or total body fat percentage as covariates in our analyses because these measures are highly correlated with certain axes—particularly the General Obesity and Muscle-Dominant axes. Adjusting for these variables could

obscure the meaningful variation in fat distribution and muscle composition that our MRI-derived phenotypes capture.

Genome-wide association studies (GWAS)

Using REGENIE version v3.1.1,(16) which is well-suited for association testing in the presence of closely related individuals, our GWAS included participants who self-identified as 'White British' who clustered with this group in PCA. We excluded participants with sex chromosome anomalies, sex discrepancies, heterozygosity outliers, and genotype call rate outliers.(17) Covariates included age, squared age, genotyping array, imaging center, and the first ten genotype-related principal components. IDPs were inverse normal transformed before analysis. Imputed SNPs, filtered by a minor allele frequency (MAF) > 0.01 and an INFO score > 0.9, resulted in 9,788,243 SNPs for the final analysis. GWAS was conducted separately for each gender, followed by a meta-analysis using METAL to integrate results across genders.

Pathway and tissue enrichment analysis

We utilized the SNP2GENE function in the Functional Mapping and Annotation (FUMA)(18) platform to identify expression quantitative trait loci (eQTLs) using GTEx v8 project.(19) Identified genes were analyzed for pathway enrichment using the PANTHER v17.0 tool,(20) enhancing our understanding of the biological pathways enriched in our gene sets.

Genetic correlation analysis

We estimated genetic correlations between obesity axes and various biomarkers, lifestyle traits, and psychological conditions using LD Score Regression (LDSC) (21). We selected 110 traits using publicly available GWAS summary statistics (**supplementary table 2**) based on established links with obesity and body composition. It is important to note that some of these GWAS include UK Biobank participants. While incorporating these datasets increases our statistical power, it may also introduce a degree of sample overlap, potentially inflating genetic correlation estimates. We set a multiple-testing-corrected significance level at $p < 0.05/110*4 = 0.00011$.

Mendelian Randomization

To investigate the potential causal impacts of different obesity axes on disease outcomes, we applied Mendelian randomization (**supplementary table 2**). Genetic variants were selected as instrumental variables for each obesity axis based on stringent criteria: a p-value of ≤ 5x10^-8 and linkage disequilibrium pruning with r^2 > 0.001 within a 10 Mb window, using European ancestry data from the 1000 Genomes Project.

Our primary method was the Inverse Variance Weighted (IVW) method. This method is subject to biases such as weak instrument bias—where the weak association between genetic instruments and exposures can skew estimates—and horizontal pleiotropy, where genetic variants may influence outcomes through pathways unrelated to the studied exposure. To try to counteract these potential biases, we

confirmed strong associations between each genetic instrument and its corresponding obesity axis (F-statistics > 10) and used MR-Egger regression to test for horizontal pleiotropy, as indicated by the Egger intercept. Additionally, we applied methods like MR-PRESSO, weighted median, simple mode, and weighted mode to enhance the robustness of our findings(22). We adjusted the results for multiple testing using the Benjamini-Hochberg correction and considered results statistically significant at an adjusted p-value < 0.05.

Results

Axes of obesity

In our study, we analyzed data from 33,122 participants who underwent MRI scanning in the UK Biobank study. We derived 24 Image-Derived Phenotypes (IDPs) from these samples, with sample characteristics detailed in **supplementary table 1**. Using these IDPs, we constructed four obesity axes through principal component analysis (PCA) performed separately for males and females. Each measure was oriented to positively correlate with BMI. The resulting obesity axes explained 4.43% to 57.50% of the variance in men and 5.89% to 54.76% in women (**supplementary figures 1 and 2)**. Consistent PC patterns across sexes allowed us to meta-analyse results for equivalent PCs (e.g., male PC1 with female PC1) (**figure 1; supplementary table 3**).

We named the axes based on their PC loadings (**figure 1**). (1) General Obesity Axis: Reflects increased fat accumulation across all regions, including visceral, subcutaneous, and ectopic fat (**figure 2A**). (2) Muscle-Dominant Axis: Indicates greater muscle volume (**figure 2B**). (3) Peripheral Fat Axis: Associated with higher subcutaneous fat in the abdominal and thigh regions (**figure 2C**). (4) Lower Body Fat Axis: Characterized by increased lower-body subcutaneous fat and reduced ectopic fat in the liver, pancreas, and muscles (**figure 2D**).

To better contextualize the axes within clinical obesity definitions, we examined the BMI distributions of individuals in the top 10% of each axis (**supplementary table 4**). Individuals in the top 10% of all axes showed significantly higher BMI ($p < 0.0001$), with most having a BMI >30 kg/m², suggesting that high scores on these axes generally reflect a phenotype consistent with clinical obesity. However, the observed differences between axes indicate that even among individuals classified as having obesity by BMI criteria, there is substantial heterogeneity in fat distribution.

Axes represent overlapping dimensions rather than discrete categories. Muscle-Dominant and Peripheral Fat Axes displayed a weak negative correlation, suggesting that individuals scoring high on one axis tend to score lower on the other (**supplementary figure 3**).

Relationship between axes and age

We analyzed the relationship between PC scores and age for all obesity axes in males and females. Scores for the General Obesity Axis increased with age (r_{men}=0.15, p_{men}<1E-10; r_{women}=0.10, p_{women}<1E-10), indicating a higher likelihood of accumulating fat in older individuals. Conversely, scores for the Muscle-Dominant (r_{men}=-0.48, p_{men}<1E-10; r_{women}=-0.36, p_{women}<1E-10), Peripheral Fat (r_{men}=-0.14, p_{men}<1E-10; r_{women}=-0.10, p_{women}<1E-10), and Lower Body Fat (r_{men}=-0.18, p_{men}<1E-10; r_{women}=-0.24, p_{women}<1E-10) Axes decreased with age, suggesting these patterns of fat or muscle distribution are less common among older individuals (**figure 3**).

Differences in axes by ancestry

To explore potential differences in the distribution of obesity axes across ancestry groups, we categorized participants into four major genetic ancestry groups: African

ancestry (N=146), Central/South Asian ancestry (N=320), East Asian ancestry (N=152), and European ancestry (N=29,179). Comparisons revealed that East Asian individuals had lower scores for the General Obesity ($p\text{-value}_{EUR\ vs\ EAS} < 0.00001$) and Lower Body Fat Axes ($p\text{-value}_{EUR\ vs\ EAS} < 0.00004$). Central/South Asians had lower scores for the Muscle-Dominant Axis ($p\text{-value}_{EUR\ vs\ CSA} < 0.00001$), while individuals of African ancestry had higher scores for the Muscle-Dominant and Lower Body Fat Axes but lower scores for the Peripheral Fat Axis (all $p\text{-value}_{EUR\ vs\ AFR} < 0.00001$, **figure 4, supplementary table 5**).

Genetic background of obesity axes

Given the ancestry-related differences in axis distribution and to minimize confounding from unrelated factors (e.g., beta-cell function differences influencing type 2 diabetes risk in individuals of African ancestry), all genetic analyses were restricted to White British participants. GWAS were conducted separately for males and females and meta-analyzed across sexes for consistent axes, resulting in a total sample size of 25,637 (**Table 1, supplementary figures 4 & 5**). No evidence of sex-specific associations was observed, as the genetic loci contributing to the axes were consistent between males and females (**supplementary table 6**).

General Obesity Axis. Two significant loci were identified: rs62033405 (eQTL for *FTO* in skeletal muscle, p-value=2.6E-7 and *IRX1* in pancreases, p-value=1.2E-7) and rs33823 (eQTL for *PEPD* in skeletal muscle; p-value=4.9e-9 and subcutaneous adipose tissue; p-value=5E-6), both previously associated with obesity-related traits. Pathway enrichment highlighted the corticosteroid receptor signaling pathway; however, these results did not remain significant after Bonferroni correction (**supplementary table 7**).

Muscle-Dominant Axis. Nine loci were associated, including rs7515497 near *FBLIM1,* rs80345488 near *RIMS2*, rs80345488 (eQTL for *RIMS2* in thyroid; p-value=7E-18), rs3850625, an exonic variant in *CACNA1S*, rs12632536 (eQTL for *DLG1* in skeletal muscle; p-value=1.2E-7), rs13170533 (sQTL for *PIK3R1* in skeletal muscle; p-value=2.2E-6), rs1028883 (eQTL for *KLF5* in skeletal muscle; p-value= 6.6e-38), rs6058093 near *PIGU* (eQTL for *GGT7*; p-value=1E-6 and *MAP1LC3A*; p-value=8E-9 in skeletal muscle), and rs9306468 near *MTMR3* (eQTL for *THOC5* in skeletal muscle*;* p-value=2E-8). Pathway enrichment analysis revealed nominally significant enrichment in pathways related to muscle function, particularly ion transport, muscle contraction, and structural integrity; however, these results did not remain significant after Bonferroni correction (**supplementary table 8**).

Peripheral Fat Axis. Fifteen loci were identified, many of which have been previously linked to WHR, lipid levels, type 2 diabetes, or red blood cell count. Three loci were shared between the Peripheral and Lower Body Fat Axes, including *COBLL1, RSPO3*, and *DNAH10/CCDC92* (**supplementary figure 6**). Pathway enrichment analysis for the Peripheral Fat Axis revealed several key pathways that provide insight into the genetic basis of this axis. These include pathways related to cellular growth and energy metabolism, which may impact adipocyte behavior, and mechanisms that regulate cell-matrix interactions and developmental processes influencing fat distribution; however, these results did not remain significant after Bonferroni correction (**supplementary table 9**).

Lower Body Fat Axis. Fifteen loci were identified, including rs1128249 (sQTL for *COBLL1* in subcutaneous fat; p-value=5E-13), rs72959041 (eQTL for *RSPO3* in subcutaneous fat; p-value=2E-8 and pQTL in blood; p-value=6E-89) rs7133378 near *DNAH10* (eQTL for *DNAH10OS* in subcutaneous fat; p-value=1E-32), rs3818717 near *RAI1* (eQTL for *TOM1L2* in subcutaneous fat; p-value=1E-15, and pQTL for SHMT1 p-value=1E-42), rs6822892 (eQTL for *PDGFC* in subcutaneous fat; p-value=3E-8), rs10406327 (eQTL for *PEPD* in subcutaneous fat; p-value=1E-11), rs2287922, an exonic variant in *RASIP1,* rs3747207 near *PNPLA3* (eQTL for *SAMM50* in subcutaneous fat; p-value=7E-15), rs2943653 near *NYAP2* (eQTL for *IRS1* in subcutaneous fat; p-value=2E-13), rs6888037 near *SLC12A2*, rs998584 near *VEGFA*, rs12138803 near *PIGC*, rs55893113 near *ZC3H11B*, rs754243 near *ANAPC1*, and rs58542926 near *TM6SF2* (pQTL for NCAN (p-value=4E-92) and SUGP1 (p-value=6E-12)). The pathway enrichment analysis indicated a significant potential role of adiponectin in metabolic regulation and the importance of lipid biosynthesis processes in maintaining healthier adipose tissue; however, these results did not remain significant after Bonferroni correction (**supplementary table 10**).

Association with metabolic biomarkers

We performed LDSC to evaluate the genetic correlations between obesity axes and a wide range of complex traits, including anthropometric measures, metabolic biomarkers, lifestyle behaviors, psychological traits, and obesity-related diseases. Out of 110 traits tested, 53 showed significant genetic correlations (corrected for multiple testing) with at least one obesity axis.

All obesity axes demonstrated positive genetic correlations with adult BMI. The General Obesity Axis showed strong positive correlations with body fat percentage, waist-to-hip ratio (WHR) in both sexes, and childhood obesity. The Muscle-Dominant Axis correlated positively with fat-free mass index, height, birth weight, and childhood obesity. The Peripheral Fat Axis was positively correlated with body fat percentage and WHR in males. In contrast, the Lower Body Fat Axis was negatively correlated with WHR in both sexes but positively associated with birth weight and childhood obesity (**figure 5a**).

Each obesity axis had distinct pattern of genetic correlation with metabolic traits and health outcomes (**figure 5b**). The General Obesity Axis showed positive correlations with insulin resistance markers, C-reactive protein (CRP), liver enzymes, branched-chain amino acids (valine, leucine, isoleucine), and triglycerides, while demonstrating negative correlations with sex hormone-binding globulin (SHBG), high-density lipoprotein cholesterol (HDL-C), and apolipoprotein A1. The Muscle-Dominant Axis did not present extensive correlations but showed a strong positive association with HOMA-IR and a negative correlation with HDL-C. The Peripheral Fat Axis correlated positively with fasting insulin and CRP levels. In contrast, the Lower Body Fat Axis was positively associated with insulin sensitivity, SHBG, and HDL-C and negatively associated with branched-chain amino acids and triglycerides.

Additionally, the General Obesity Axis was positively correlated with sedentary behavior, smoking, Attention-Deficit/Hyperactivity Disorder (ADHD), substance use, and binge eating. Conversely, the Muscle-Dominant Axis was negatively correlated with sleep duration, while the Peripheral Fat Axis was negatively correlated with

physical activity (**figure 5c**). These findings underscore the complex and distinct metabolic and lifestyle associations for each obesity axis.

Association with disease outcomes

In our UK Biobank imaging sub-cohort, the General Obesity Axis was associated with a higher risk of various cardiovascular diseases, asthma, psoriasis, and depression but a lower risk of osteoporosis. In contrast, the Lower Body Fat Axis was associated with a lower risk of cardiovascular diseases. For example, participants in the top 10% of the General Obesity Axis, as determined by their PC scores, had approximately 25% (95% confidence interval: 22% to 29%) higher odds of developing type 2 diabetes compared to those in the bottom 10% based on prevalent disease cases. Conversely, individuals in the top 10% for the Lower Body Fat Axis had 55% lower odds (95% CI: 50% to 60%) of developing type 2 diabetes compared to those in the bottom 10% (**supplementary figure 7**).

To validate these findings in studies independent of the UK Biobank dataset, we performed genetic correlation analyses between the obesity axes and disease risks. The General Obesity Axis was genetically correlated with a higher risk of type 2 diabetes, steatotic liver disease, hypertension, coronary heart disease, stroke, myocardial infarction, aortic aneurysm, heart failure, peripheral artery disease, gout, osteoarthritis, asthma, psoriasis, depression, and cholelithiasis. The Muscle-Dominant Axis was linked to a higher risk of type 2 diabetes, chronic kidney disease, atrial fibrillation, and osteoarthritis but a lower risk of depression. The Peripheral Fat Axis did not present significant genetic correlations with major diseases. The Lower Body Fat Axis was associated with a lower risk of type 2 diabetes, steatotic liver disease, and myocardial infarction (**figure 5d**).

Mendelian randomization analyses, using genetic instruments with robust F-statistics (F = 36 for the General Obesity Axis, F = 31 for the Muscle-Dominant Axis, F = 42 for the Peripheral Fat Axis, and F = 40 for the Lower Body Fat Axis), provided support for causal associations between obesity axes and various disease outcomes (**figure 6; supplementary table 11**). The General Obesity Axis, was instrumented with only two variants, and therefore, sensitivity tests such as MR-Egger could not be reliably performed; our conclusions for this axis are based solely on IVW estimates, which linked it to increased risks of osteoarthritis, asthma, cholelithiasis, and gastroesophageal reflux disease. For the Muscle-Dominant Axis, while IVW indicated an increased risk of chronic kidney disease and osteoarthritis, the association with hip osteoarthritis did not replicate in the MR-Egger analysis. For the Peripheral Fat Axis, sensitivity tests were generally consistent, except that MR-Egger did not confirm associations with chronic kidney disease, steatotic liver disease, and polycystic ovary syndrome. Finally, for the Lower Body Fat Axis, the majority of MR sensitivity tests corroborated IVW findings—linking this axis to lower risks of type 2 diabetes, polycystic ovary syndrome, steatotic liver disease, hypertension, myocardial infarction, aortic aneurysm, and psoriasis, and a higher risk of osteoarthritis—except MR-Egger estimates which failed to replicate associations for aortic aneurysm and coronary heart disease.

Discussion

This study presents a comprehensive exploration of obesity, leveraging advanced imaging and genetic analyses to unravel the complex pathways underlying obesity. Using MRI-derived phenotypes from the UK Biobank, we identified four distinct axes of obesity: General Obesity, Muscle-Dominant, Peripheral Fat, and Lower Body Fat. These findings highlight the heterogeneity of obesity and underscore some limitations of conventional metrics like BMI in capturing the nuances of individual obesity-related risks and outcomes.

Implications of axes for disease risk

The identification of these axes provides important insights into disease mechanisms. The General Obesity Axis, characterized by overall fat accumulation, was strongly associated with increased risks for several metabolic and cardiovascular conditions, including type 2 diabetes, hypertension, myocardial infarction, and liver disease. These findings align with prior research linking overall adiposity to metabolic dysregulation and inflammation(23, 24). Pathway enrichment analyses suggest a role for corticosteroid receptor signaling, though the extent of its direct contribution remains uncertain. While elevated cortisol levels, as seen in conditions like Cushing's syndrome(25), are clearly implicated in metabolic disturbances, other factors likely play a more prominent role in general obesity.

The Muscle-Dominant Axis, defined by increased muscle volume, presented a unique metabolic profile. While higher HOMA-IR levels were observed, there was no association with other insulin sensitivity indices, suggesting insulin resistance might be confined to specific tissues such as the liver. The increased risks of chronic kidney disease and atrial fibrillation, coupled with a lower risk of depression, highlight the complexity of this axis. Previous studies have shown that increased muscle mass can have both beneficial and detrimental metabolic effects, depending on factors such as muscle composition and lipid infiltration(26, 27). The elevated risks of chronic kidney disease and atrial fibrillation might indicate a link between higher muscle mass and increased cardiac workload, as well as renal strain due to increased protein metabolism and creatinine turnover. The lower risk of depression associated with this axis supports previous findings that greater muscle mass may be protective against mood disorders, potentially through improved physical function and self-perception(28). Genetic loci associated with the Muscle-Dominant Axis, including *CACNA1S*, *DLG1*, and *PIK3R1*, further point to the importance of muscle function, ion transport, and insulin signaling in this phenotype.

The Peripheral Fat Axis, associated with higher subcutaneous fat in the abdomen and thighs, demonstrated a relatively benign metabolic profile, with no significant genetic correlation with major disease outcomes. This finding aligns with previous studies indicating that subcutaneous fat, particularly in peripheral regions, is less metabolically detrimental than visceral fat(29-32). This contrasts with the General Obesity Axis, highlighting that not all forms of fat accumulation carry the same health risks.

The Lower Body Fat Axis, marked by increased lower body subcutaneous fat and reduced ectopic fat, exhibited a favorable metabolic profile. Participants with higher scores along this axis showed lower risks of type 2 diabetes, myocardial infarction,

and fatty liver disease. These findings support the protective metabolic effects of gluteofemoral fat as a “safe storage depot”, consistent with previous genetic studies(24, 31, 33, 34). Pathway enrichment analyses highlighted the importance of adiponectin secretion and lipid biosynthesis, suggesting enhanced adipocyte function and fat storage capacity may drive this protective effect.

Ancestry-related differences and precision medicine

Significant ancestry-related variations in the distribution of these axes were observed. For example, East Asian participants had lower scores for the General and Lower Body Fat Axes, while African participants exhibited higher scores for the Muscle-Dominant and Lower Body Fat Axes but lower scores for the Peripheral Fat Axis. These differences underscore the need for ancestry-informed approaches in managing obesity and its associated disease risks. The metabolic risks tied to each axis may vary across populations, emphasizing the importance of moving beyond a "one-size-fits-all" strategy in obesity management(9, 35).

Genetic insights

The GWAS identified distinct genetic loci and pathways associated with each axis, providing novel insights into the biological mechanisms underlying fat distribution patterns. For the Muscle-Dominant Axis, several genes of particular interest were identified. *CACNA1S* has been linked to mild human myopathy, with supporting evidence from zebrafish models.(36) Disruptions in *DLG1*, which impair myosin distribution, can affect muscle efficiency and metabolic regulation(37). *PIK3R1* is critical in muscle metabolism, as demonstrated by knockout mice that resist glucocorticoid-induced insulin resistance and muscle atrophy, maintaining healthier muscle structure(38). *KLF5*, a zinc-finger transcription factor, is essential for cell proliferation and muscle regeneration(39). *GGT7* plays a key role in glutathione metabolism, protecting against oxidative stress and supporting muscle health(40). *MAP1LC3A* is involved in the autophagy pathway essential for muscle repair(41). *THOC5* influences muscle differentiation and haematopoiesis(42).

Genes highlighted for Lower Body Fat Axis have been previously shown to be involved in adipose tissue function. Knocking down *COBLL1* disrupts fat storage by impairing stress fiber breakdown in subcutaneous fat cells, affecting insulin responsiveness and lipid metabolism.(43) Variants in *RSPO3* suppress adipogenesis, promote apoptosis of gluteal adipocytes, limit adipose tissue expansion, and stimulate upper-body fat distribution(44). *DNAH10OS* regulates nearby genes like *DNAH10* and *CCDC92*, both involved in lipid accumulation in adipocyte models(45). SHMT2 deficiency in mice increases fatty liver, highlighting its role in fat metabolism(46). *PDGFC* regulates adipose tissue in response to dietary changes(47). *PEPD* is vital for collagen turnover in adipose tissue, with lower expression linked to increased fibrosis and insulin resistance(48). *RASIP1* plays a crucial role in vascular development and endothelial cell function, which are integral to the health and function of adipose tissue(49). *SAMM50* is involved in beige adipocyte thermogenesis and energy balance(50). Shared genetic architecture between the Peripheral Fat and Lower Body Fat Axes, including genes like *RSPO3, COBLL1*, and *DNAH10OS*, points to overlapping mechanisms. Additionally, genes involved in adipogenesis, lipid metabolism, and insulin signaling emerged as key

drivers of these axes. Tissue-specific eQTLs in skeletal muscle and adipose tissue further underscore the role of regulatory mechanisms in shaping these phenotypes.

Clinical implications and future directions

Our study provides novel insights into the heterogeneity of obesity by leveraging MRI-derived phenotypes to define distinct obesity axes. Unlike traditional measures such as BMI(2), our approach offers a more granular assessment of body composition and its genetic determinants, revealing that individuals with similar BMIs can present vastly different patterns of fat distribution and metabolic risk. We show that these axes have distinct genetic backgrounds, with no evidence of sex-specific associations, suggesting that genetic influences on fat distribution and muscle volume are largely shared between men and women. Although many of the genetic markers we identified have been previously implicated in adiposity, our findings, such as the associations linking *RSPO3* and *COBLL1* to the Lower Body Fat Axis and unique loci for the Muscle-Dominant Axis, underscore the complexity of obesity and suggest that the underlying biological mechanisms differ across these axes.

While these findings are not yet directly applicable in clinical practice, they lay the groundwork potentially for future precision medicine approaches. As imaging technologies become more accessible, MRI-derived obesity classifications may eventually allow for targeted interventions that address specific patterns of fat distribution and muscle composition. Furthermore, our study highlights the potential value for risk stratification beyond BMI, as even individuals classified as living with obesity by conventional standards may have different disease trajectories. Also, understanding the genetic architecture of these obesity axes may guide therapeutic research, particularly in developing treatments that modulate fat storage patterns or muscle composition to mitigate metabolic risk. Future work should focus on replicating these findings in more diverse populations and on investigating whether these obesity axes predict incident disease risk over time, ultimately guiding the development of tailored therapeutic strategies. How newer weight loss therapies influence body compositional changes and future outcome risks in these different obesity phenotypes will also be of interest.

Strengths and Limitations:

This study's strengths include its large sample size and the use of advanced MRI imaging to define obesity axes. However, limitations include the restriction of analyses to individuals of White British ancestry, which may affect the generalizability of the findings to other populations. Future studies should replicate these findings in more diverse cohorts. Additionally, while Mendelian randomization provided causal insights, potential residual confounding or pleiotropic effects cannot be completely ruled out.

Conclusion:

This study highlights the complexity and heterogeneity of obesity by identifying distinct axes with unique genetic, metabolic, and disease risk profiles. Potentially extending beyond BMI and integrating advanced imaging with multi-omics data provides a nuanced understanding of obesity. These findings pave the way for more

personalized approaches to obesity treatment and prevention, tailored to an individual's genetic, metabolic, and fat distribution profile.

Financial support statement
H.Y. is funded by Diabetes UK (grant 23/0006598). C.O. and H.Y. are funded by Calico Life Sciences LLC.

Author Contributions and Guarantor Statement
C.O. and A.N. analysed the data. H.Y. designed the study and wrote the manuscript. M.C., B.W., M.J., E.L.T. and J.D.B. provided all the MRI-derived IDPs. M.C. performed the genome-wide association studies. N.S. and all authors contributed to the reviewing, editing and approving the manuscript. H.Y. is the guarantor of this work and, as such, has full access to all the data in the study and takes responsibility for the integrity of the data and the accuracy of the data analysis.

Data availability
Our research was conducted using UK Biobank data. Under the standard UK Biobank data sharing agreement, we (and other researchers) cannot directly share raw data obtained or derived from the UK Biobank. However, under this agreement, all of the data generated, and methodologies used in this paper are returned by us to the UK Biobank, where they will be fully available. Access can be obtained directly from the UK Biobank to all bona fide researchers upon submitting a health-related research proposal to the UK Biobank https://www.ukbiobank.ac.uk.

Acknowledgments
This research was conducted using the UK Biobank Resource under Application Number 44584. We also want to acknowledge the participants and investigators of the FinnGen study.

Conflict of interest
N.S. has received grant and personal fees from AstraZeneca, Boehringer Ingelheim, and Novartis; a grant from Roche Diagnostics; and personal fees from Abbott Laboratories, Afimmune, Amgen, Eli Lilly, Hanmi Pharmaceuticals, Merck Sharp & Dohme, Novo Nordisk, Pfizer, and Sanofi outside the submitted work. M.C. and E.S. are employees of Calico Life Sciences LLC. C.S.O, A.N., M.T., B.W., J.D.B., E.L.T., and H.Y. reported no conflict of interest relevant to this article.

Table 1. Genetic results for the different obesity axes.

Obesity Axes	rsID	Chr	Position	P	EA	NEA	Beta	Se	Nearest Gene	Locus previously associated with
General Obesity	rs62033405	16	53822387	5.6E-11	T	C	0.06	0.01	*FTO*	Obesity and metabolic traits
General Obesity	rs33823	19	34000725	8.2E-10	T	C	0.06	0.01	*PEPD*	Obesity and metabolic traits
Muscle-Dominant	rs7515497	1	16120240	2.6E-8	T	G	-0.04	0.01	*FBLIM1*	-
Muscle-Dominant	rs3850625	1	201016296	4.5E-8	A	G	-0.07	0.01	*CACNA1S*	Lean mass, creatinine, estimated glomerular filtration rate, lung function and liver enzymes
Muscle-Dominant	rs2138157	2	227103717	1.4E-8	A	C	-0.05	0.01	*IRS1*	Lipids, obesity, and other metabolic biomarkers
Muscle-Dominant	rs12632536	3	196833650	4E-9	T	C	-0.05	0.01	*DLG1*	Lung function, creatinine and estimated glomerular filtration rate
Muscle-Dominant	rs13170533	5	68058041	4.6E-9	C	G	-0.08	0.01	*SLC30A5*	Creatinine levels, estimated glomerular filtration rate and lung function
Muscle-Dominant	rs80345488	8	104536643	4.7E-8	A	C	0.10	0.02	*RIMS2*	-
Muscle-Dominant	rs1028883	13	74108587	4.2E-9	T	G	-0.05	0.01	*KLF5*	Lean mass, liver enzyme levels, and kidney function
Muscle-Dominant	rs6058093	20	33213196	3.2E-10	A	C	0.05	0.01	*PIGU*	Estimated glomerular filtration rate, liver enzymes, creatinine levels, and lung function
Muscle-Dominant	rs9306468	22	30374281	4.7E-9	T	C	0.05	0.01	*MTMR3*	Lung function, estimated glomerular filtration rate, and creatinine levels

Peripheral Fat	rs11205797	1	51474198	2.9E-9	A	G	-0.05	0.01	*CDKN2C*	Red blood cell count
Peripheral Fat	rs566596164	2	165558215	4.2E-12	C	G	0.09	0.01	*COBLL1*	WHR, lipids, type 2 diabetes, other metabolic biomarkers
Peripheral Fat	rs13172689	5	53463520	3.2E-10	A	G	-0.07	0.01	*ARL15*	Type 2 diabetes
Peripheral Fat	rs1651274	5	158020425	3.3E-8	A	G	-0.06	0.01	*EBF1*	WHR, lipids, type 2 diabetes, other metabolic biomarkers
Peripheral Fat	rs141783576	6	127439897	4.5E-12	C	G	-0.12	0.02	*RSPO3*	WHR, lipids, type 2 diabetes, other metabolic biomarkers
Peripheral Fat	rs10827616	10	36469937	1E-9	T	C	0.05	0.01	*FZD8*	Red blood cell count
Peripheral Fat	rs7129492	11	74381181	2.1E-12	A	G	-0.06	0.01	*POLD3*	Colorectal cancer, creatinine
Peripheral Fat	rs11045236	12	20578939	3E-9	T	C	-0.06	0.01	*PDE3A*	White blood cell count, lipids, HbA1c
Peripheral Fat	rs11057413	12	124489162	2.9E-9	A	G	-0.05	0.01	*ZNF664, FAM101A*	WHR, lipids, type 2 diabetes, other metabolic biomarkers
Peripheral Fat	rs749170	13	22350875	3.3E-10	T	C	-0.06	0.01	*FGF9*	Platelet count, SHBG, liver enzyme
Peripheral Fat	rs3116602	13	51111355	5.1E-12	T	G	-0.07	0.01	*DLEU1*	WHR, lipids
Peripheral Fat	rs9565581	13	81098500	2.5E-13	A	C	-0.07	0.01	*SPRY2*	Body fat
Peripheral Fat	rs1883711	20	39179822	1.5E-9	C	G	-0.15	0.02	*SNORD112*	Lipids, metabolic biomarkers
Peripheral Fat	rs11698277	20	45502865	5.3E-14	T	C	-0.07	0.01	*EYA2*	WHR
Peripheral Fat	rs2267373	22	38600542	1.9E-12	T	C	-0.06	0.01	*PLA2G6, MAFF*	WHR, lipids, type 2 diabetes, other metabolic biomarkers
Lower Body Fat	rs12138803	1	172348823	3.1E-8	T	C	-0.05	0.01	*DNM3, PIGC*	WHR and SHBG
Lower Body Fat	rs55893113	1	219773122	8E-9	C	G	0.05	0.01	*ZC3H11B*	WHR, SHBG, lipids and type 2 diabetes

Lower Body Fat	rs754243	2	112251121	7.1E-10	A	G	0.06	0.01	*ANAPC1*	WHR, SHBG
Lower Body Fat	rs1128249	2	165528624	1.1E-17	T	G	0.07	0.01	*COBLL1*	Lipids, obesity, type 2 diabetes and other metabolic biomarkers
Lower Body Fat	rs2943653	2	227047771	1.1E-9	T	C	-0.05	0.01	*NYAP2*	Lipids, type 2 diabetes and metabolic biomarkers
Lower Body Fat	rs6822892	4	157734675	2.3E-8	A	G	-0.05	0.01	*PDGFC*	Lipids, type 2 diabetes and metabolic biomarkers
Lower Body Fat	rs6888037	5	127406259	2.2E-8	T	G	-0.05	0.01	*SLC12A2*	Lipids, measures of obesity and metabolic biomarkers
Lower Body Fat	rs998584	6	43757896	2.1E-18	A	C	-0.07	0.01	*VEGFA*	WHR, lipids, type 2 diabetes and metabolic biomarkers
Lower Body Fat	rs72959041	6	127454893	5.6E-11	A	G	-0.13	0.02	*RSPO3*	WHR and lipids
Lower Body Fat	rs7133378	12	124409502	1.6E-11	A	G	0.06	0.01	*DNAH10, CCDC92*	WHR, lipids, and type 2 diabetes
Lower Body Fat	rs3818717	17	17707105	1.3E-8	T	C	-0.05	0.01	*RAI1*	WHR, lipids, and type 2 diabetes
Lower Body Fat	rs58542926	19	19379549	3.5E-19	T	C	-0.14	0.02	*TM6SF2*	Lipids and type 2 diabetes
Lower Body Fat	rs10406327	19	33890838	5.9E-9	C	G	0.05	0.01	*PEPD*	WHR and type 2 diabetes
Lower Body Fat	rs2287922	19	49232226	2.3E-8	A	G	-0.05	0.01	*RASIP1*	WHR, lipids, and other metabolic biomarkers
Lower Body Fat	rs3747207	22	44324855	3.5E-30	A	G	-0.12	0.01	*PNPLA3*	Liver enzymes, fatty liver, lipids and type 2 diabetes

Chr: chromosome; P: p-value; EA: effect allele; NEA: non-effect allele; Se: standard error

Figure legends.

Figure 1. Characteristics of Obesity Axes.

Radial plots display the magnitudes of principal component (PC) loadings for the four obesity axes from (A) men and (B) women. Points above the inner circle indicate positive loadings, reflecting traits that contribute positively to the respective obesity axis, whereas points below the inner circle represent negative loadings, indicating traits that contribute inversely to the axis.

Figure 2. MRI Scans and Fat Distribution Patterns Across Obesity Axes.

MRI scans illustrate the contrasting fat distribution patterns observed in individuals with the highest and lowest scores along each obesity axis. These visual comparisons highlight the distinctive anatomical fat accumulation and muscle distribution associated with each axis.

Figure 3. Relationship Between Obesity Axes and Age in (A) Males and (B) Females.

Scatter plots depict the variation in scores for each obesity axis across different ages. General obesity scores tend to increase with age, while scores for other axes, such as the Lower Body Fat Axis, decrease in older individuals.

Figure 4. Ancestry-related Variation in Obesity Axes.
Density plots show the distribution of scores for each obesity axis across different ancestry groups. AFR = African ancestry, CSA = Central/South Asian ancestry, EAS = East Asian ancestry, EUR = European ancestry.

Figure 5. Genetic Correlations Between Obesity Axes and Selected biomarkers, Lifestyle Traits and Psychological Disorders.

Heatmap of genetic correlations (rg) between obesity axes and (a) anthropometric traits, insulin-related traits, and metabolic biomarkers, (b) metabolites, (c) lifestyle traits and psychological disorders; and (d) various disease outcomes, including cardiovascular disease and type 2 diabetes. Colors and their intensities represent the correlation coefficients (rg), with asterisks indicating statistical significance after multiple testing correction (p-value < 0.00011).

Figure 6. **Mendelian randomization.**

The heatmap illustrates causal associations between obesity axes and selected disease outcomes. Colors and their intensities represent the direction and strength of associations determined by the Inverse Variance Weighted (IVW) method. Asterisks indicate statistical significance after Benjamini-Hochberg correction (adjusted p-value < 0.05).

References

1. Elmaleh-Sachs A, Schwartz JL, Bramante CT, Nicklas JM, Gudzune KA, Jay M. Obesity Management in Adults: A Review. JAMA. 2023;330(20):2000-15.
2. Abraham A, Yaghootkar H. Identifying obesity subtypes: A review of studies utilising clinical biomarkers and genetic data. Diabetic Medicine. 2023;40(12):e15226.
3. Bray GA. Medical Consequences of Obesity. The Journal of Clinical Endocrinology & Metabolism. 2004;89(6):2583-9.
4. Perdomo CM, Cohen RV, Sumithran P, Clément K, Frühbeck G. Contemporary medical, device, and surgical therapies for obesity in adults. The Lancet. 2023;401(10382):1116-30.
5. Pillon NJ, Loos RJF, Marshall SM, Zierath JR. Metabolic consequences of obesity and type 2 diabetes: Balancing genes and environment for personalized care. Cell. 2021;184(6):1530-44.
6. Zhou Z, Macpherson J, Gray SR, Gill JMR, Welsh P, Celis-Morales C, et al. Are people with metabolically healthy obesity really healthy? A prospective cohort study of 381,363 UK Biobank participants. Diabetologia. 2021;64(9):1963-72.
7. Ahima RS, Lazar MA. The health risk of obesity—better metrics imperative. Science. 2013;341(6148):856-8.
8. Bodaghi A, Fattahi N, Ramazani A. Biomarkers: Promising and valuable tools towards diagnosis, prognosis and treatment of Covid-19 and other diseases. Heliyon. 2023;9(2).
9. Yaghootkar H, Whitcher B, Bell JD, Thomas EL. Ethnic differences in adiposity and diabetes risk – insights from genetic studies. Journal of Internal Medicine. 2020;288(3):271-83.
10. Littlejohns TJ, Holliday J, Gibson LM, Garratt S, Oesingmann N, Alfaro-Almagro F, et al. The UK Biobank imaging enhancement of 100,000 participants: rationale, data collection, management and future directions. Nature communications. 2020;11(1):2624.
11. Basty N, Liu Y, Cule M, Thomas EL, Bell JD, Whitcher B, editors. Automated measurement of pancreatic fat and iron concentration using multi-echo and T1-weighted MRI data2020 2020: IEEE.
12. Liu Y, Basty N, Whitcher B, Bell JD, Sorokin EP, van Bruggen N, et al. Genetic architecture of 11 organ traits derived from abdominal MRI using deep learning. Elife. 2021;10:e65554.
13. Whitcher B, Thanaj M, Cule M, Liu Y, Basty N, Sorokin EP, et al. Precision MRI phenotyping enables detection of small changes in body composition for longitudinal cohorts. Scientific Reports. 2022;12(1):3748.
14. Thanaj M, Basty N, Whitcher B, Sorokin EP, Liu Y, Srinivasan R, et al. Precision MRI phenotyping of muscle volume and quality at a population scale. Frontiers in Physiology. 2024;15:1288657.
15. Bydder M, Ghodrati V, Gao Y, Robson MD, Yang Y, Hu P. Constraints in estimating the proton density fat fraction. Magnetic resonance imaging. 2020;66:1-8.
16. Mbatchou J, Barnard L, Backman J, Marcketta A, Kosmicki JA, Ziyatdinov A, et al. Computationally efficient whole-genome regression for quantitative and binary traits. Nature genetics. 2021;53(7):1097-103.
17. Bycroft C, Freeman C, Petkova D, Band G, Elliott LT, Sharp K, et al. The UK Biobank resource with deep phenotyping and genomic data. Nature. 2018;562(7726):203-9.

18. Watanabe K, Taskesen E, Van Bochoven A, Posthuma D. Functional mapping and annotation of genetic associations with FUMA. Nature communications. 2017;8(1):1826.
19. Consortium GT. The GTEx Consortium atlas of genetic regulatory effects across human tissues. Science. 2020;369(6509):1318-30.
20. Thomas PD, Ebert D, Muruganujan A, Mushayahama T, Albou LP, Mi H. PANTHER: Making genome-scale phylogenetics accessible to all. Protein Science. 2022;31(1):8-22.
21. Bulik-Sullivan B, Finucane HK, Anttila V, Gusev A, Day FR, Loh P-R, et al. An atlas of genetic correlations across human diseases and traits. Nature Genetics. 2015;47(11):1236-41.
22. Burgess S, Thompson SG. Interpreting findings from Mendelian randomization using the MR-Egger method. European journal of epidemiology. 2017;32:377-89.
23. Magkos F, Sørensen TIA, Raubenheimer D, Dhurandhar NV, Loos RJF, Bosy-Westphal A, et al. On the pathogenesis of obesity: causal models and missing pieces of the puzzle. Nat Metab. 2024;6(10):1856-65.
24. Martin S, Tyrrell J, Thomas EL, Bown MJ, Wood AR, Beaumont RN, et al. Disease consequences of higher adiposity uncoupled from its adverse metabolic effects using Mendelian randomisation. Elife. 2022;11.
25. Pivonello R, De Martino MC, De Leo M, Simeoli C, Colao A. Cushing's disease: the burden of illness. Endocrine. 2017;56(1):10-8.
26. Kim G, Lee SE, Jun JE, Lee YB, Ahn J, Bae JC, et al. Increase in relative skeletal muscle mass over time and its inverse association with metabolic syndrome development: a 7-year retrospective cohort study. Cardiovasc Diabetol. 2018;17(1):23.
27. Thanaj M, Basty N, Whitcher B, Sorokin EP, Liu Y, Srinivasan R, et al. Precision MRI phenotyping of muscle volume and quality at a population scale. Front Physiol. 2024;15:1288657.
28. Wang Z, Wu M, Shao X, Yang Q. Muscle quality index is associated with depression among non-elderly US adults. BMC Psychiatry. 2024;24(1):672.
29. Yaghootkar H, Scott RA, White CC, Zhang W, Speliotes E, Munroe PB, et al. Genetic evidence for a normal-weight "metabolically obese" phenotype linking insulin resistance, hypertension, coronary artery disease, and type 2 diabetes. Diabetes. 2014;63(12):4369-77.
30. Yaghootkar H, Lotta LA, Tyrrell J, Smit RA, Jones SE, Donnelly L, et al. Genetic Evidence for a Link Between Favorable Adiposity and Lower Risk of Type 2 Diabetes, Hypertension, and Heart Disease. Diabetes. 2016;65(8):2448-60.
31. Lotta LA, Gulati P, Day FR, Payne F, Ongen H, van de Bunt M, et al. Integrative genomic analysis implicates limited peripheral adipose storage capacity in the pathogenesis of human insulin resistance. Nat Genet. 2017;49(1):17-26.
32. Ji Y, Yiorkas AM, Frau F, Mook-Kanamori D, Staiger H, Thomas EL, et al. Genome-Wide and Abdominal MRI Data Provide Evidence That a Genetically Determined Favorable Adiposity Phenotype Is Characterized by Lower Ectopic Liver Fat and Lower Risk of Type 2 Diabetes, Heart Disease, and Hypertension. Diabetes. 2019;68(1):207-19.
33. Abraham A, Cule M, Thanaj M, Basty N, Hashemloo MA, Sorokin EP, et al. Genetic Evidence for Distinct Biological Mechanisms That Link Adiposity to Type 2 Diabetes: Toward Precision Medicine. Diabetes. 2024;73(6):1012-25.

34. Martin S, Cule M, Basty N, Tyrrell J, Beaumont RN, Wood AR, et al. Genetic Evidence for Different Adiposity Phenotypes and Their Opposing Influences on Ectopic Fat and Risk of Cardiometabolic Disease. Diabetes. 2021;70(8):1843-56.
35. Ahmed A, Justo S, Yaghootkar H. Genetic scores associated with favourable and unfavourable adiposity have consistent effect on metabolic profile and disease risk across diverse ethnic groups. Diabet Med. 2023;40(12):e15213.
36. Endo Y, Groom L, Wang SM, Pannia E, Griffiths NW, Van Gennip JLM, et al. Two zebrafish cacna1s loss-of-function variants provide models of mild and severe CACNA1S-related myopathy. Human Molecular Genetics. 2024;33(3):254-69.
37. Fuentes MA, Piper HN, He B. Dlg1 regulates subcellular distribution of non-muscle myosin II during Drosophila germband extension. bioRxiv. 2022:2022-08.
38. Chen T-C, Kuo T, Dandan M, Lee RA, Chang M, Villivalam SD, et al. The role of striated muscle Pik3r1 in glucose and protein metabolism following chronic glucocorticoid exposure. Journal of Biological Chemistry. 2021;296.
39. Hayashi S, Manabe I, Suzuki Y, Relaix F, Oishi Y. Klf5 regulates muscle differentiation by directly targeting muscle-specific genes in cooperation with MyoD in mice. Elife. 2016;5:e17462.
40. Baldelli S, Ciccarone F, Limongi D, Checconi P, Palamara AT, Ciriolo MR. Glutathione and nitric oxide: key team players in use and disuse of skeletal muscle. Nutrients. 2019;11(10):2318.
41. Carnio S, LoVerso F, Baraibar MA, Longa E, Khan MM, Maffei M, et al. Autophagy impairment in muscle induces neuromuscular junction degeneration and precocious aging. Cell reports. 2014;8(5):1509-21.
42. Saran S, Tran DDH, Klebba-Färber S, Moran-Losada P, Wiehlmann L, Koch A, et al. THOC5, a member of the mRNA export complex, contributes to processing of a subset of wingless/integrated (Wnt) target mRNAs and integrity of the gut epithelial barrier. BMC Cell Biology. 2013;14:1-14.
43. Glunk V, Laber S, Sinnott-Armstrong N, Sobreira DR, Strobel SM, Batista TM, et al. A non-coding variant linked to metabolic obesity with normal weight affects actin remodelling in subcutaneous adipocytes. Nature Metabolism. 2023;5(5):861-79.
44. Loh NY, Minchin JEN, Pinnick KE, Verma M, Todorčević M, Denton N, et al. RSPO3 impacts body fat distribution and regulates adipose cell biology in vitro. Nature communications. 2020;11(1):2797.
45. Lotta LA, Gulati P, Day FR, Payne F, Ongen H, Van De Bunt M, et al. Integrative genomic analysis implicates limited peripheral adipose storage capacity in the pathogenesis of human insulin resistance. Nature genetics. 2017;49(1):17-26.
46. Chen G, Zhou G, Zhai L, Bao X, Tiwari N, Li J, et al. SHMT2 reduces fatty liver but is necessary for liver inflammation and fibrosis in mice. Communications Biology. 2024;7(1):173.
47. Cox N, Crozet L, Holtman IR, Loyher P-L, Lazarov T, White JB, et al. Diet-regulated production of PDGFcc by macrophages controls energy storage. Science. 2021;373(6550):eabe9383.
48. Pellegrinelli V, Rodriguez-Cuenca S, Rouault C, Figueroa-Juarez E, Schilbert H, Virtue S, et al. Dysregulation of macrophage PEPD in obesity determines adipose tissue fibro-inflammation and insulin resistance. Nature metabolism. 2022;4(4):476-94.
49. Lee M, Betz C, Yin J, Paatero I, Schellinx N, Carte AN, et al. Control of dynamic cell behaviors during angiogenesis and anastomosis by Rasip1. Development. 2021;148(15):dev197509.

50. Park S-J, Shon D-H, Kim J-H, Ryu Y-H, Ko Y. SAMM50 regulates thermogenesis of beige adipocytes differentiated from human adipose-derived stem cells by balancing mitochondrial dynamics. International journal of molecular sciences. 2022;23(12):6764.

Figure 1A

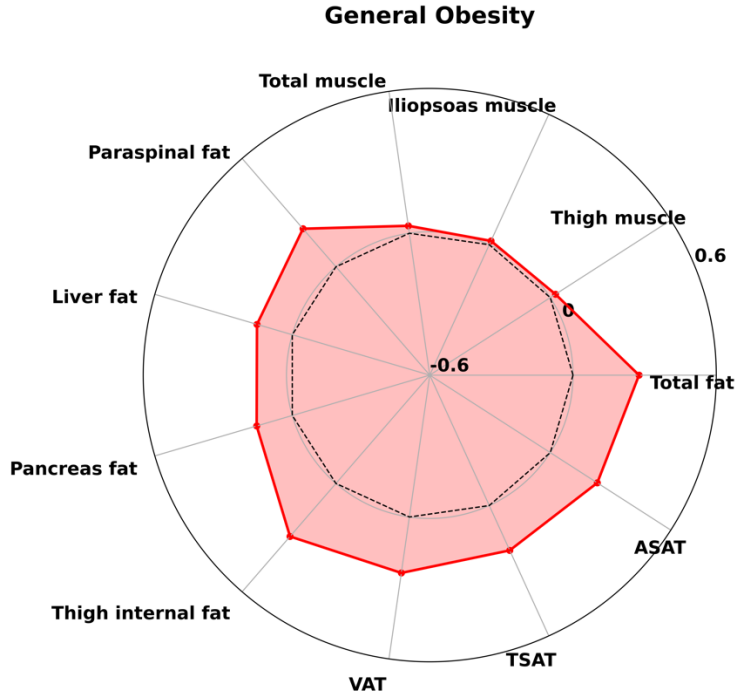

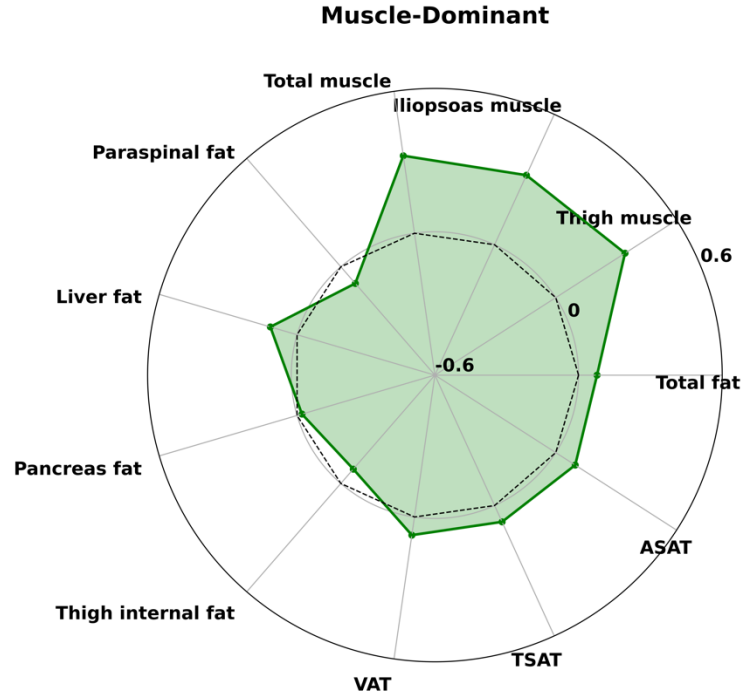

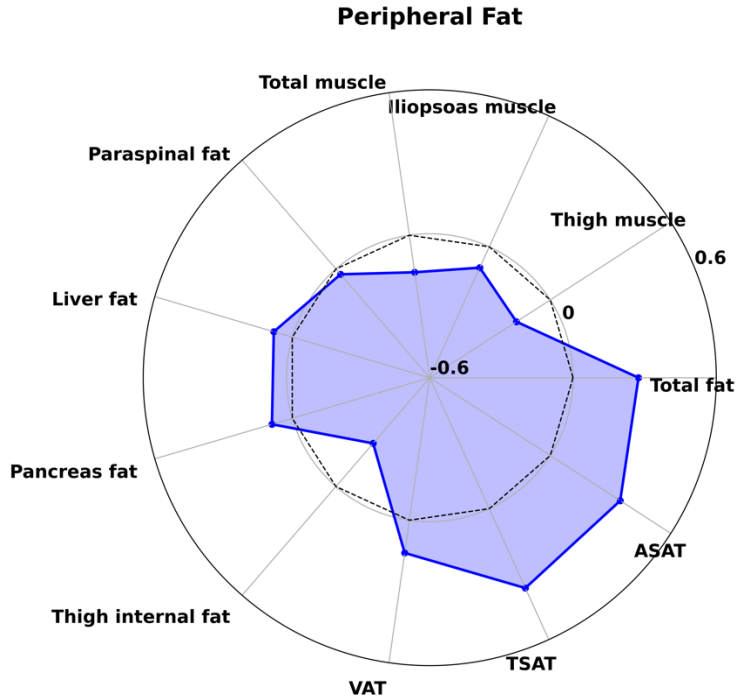

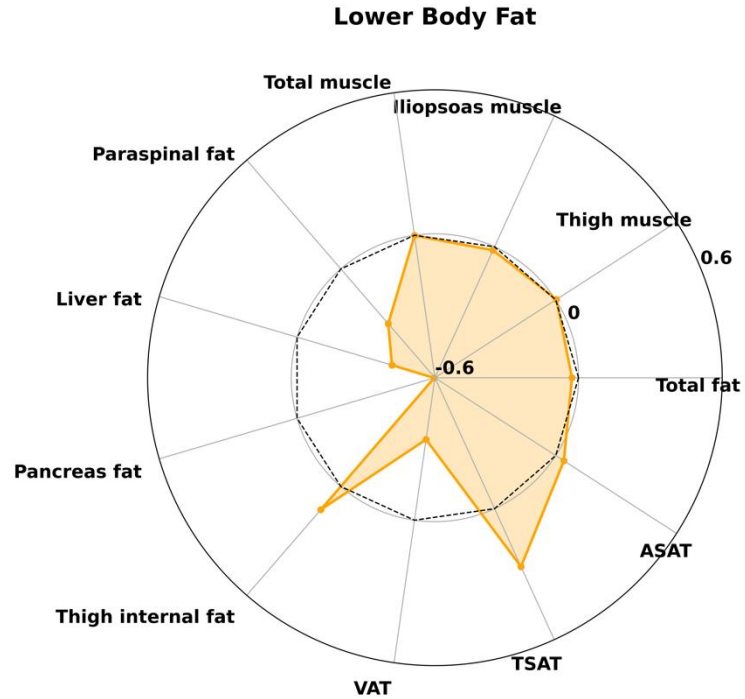

Figure 1B

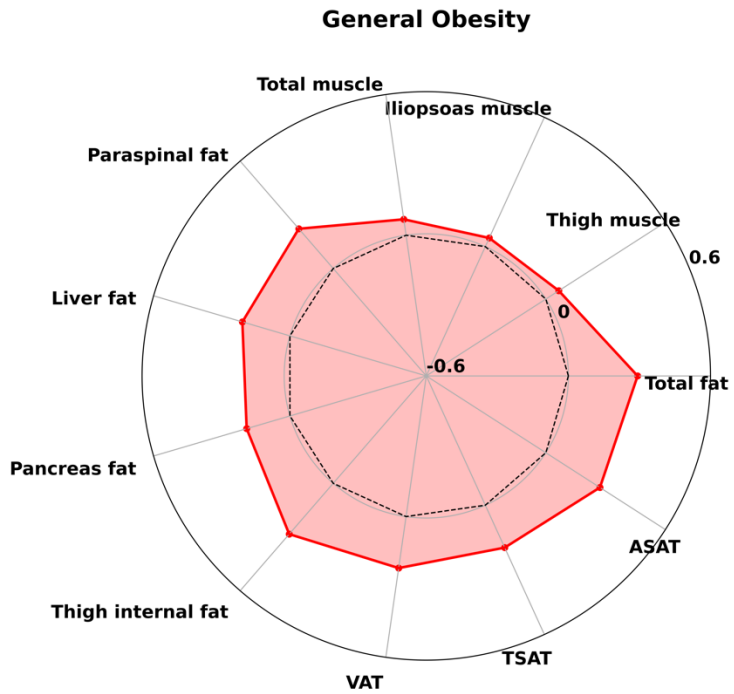

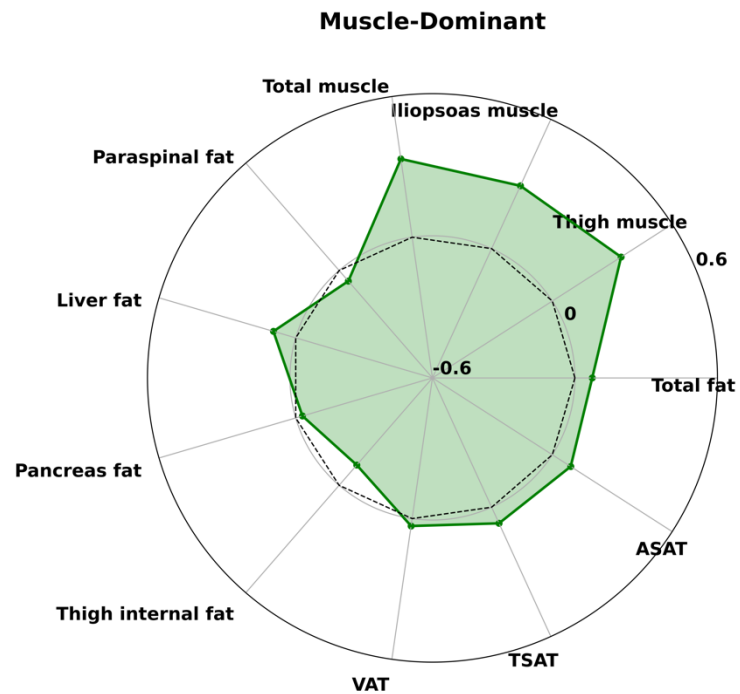

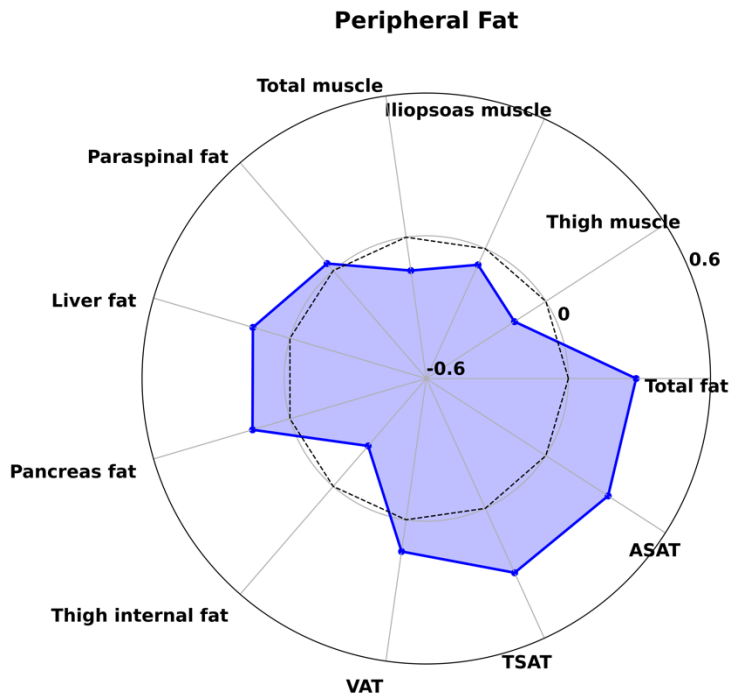

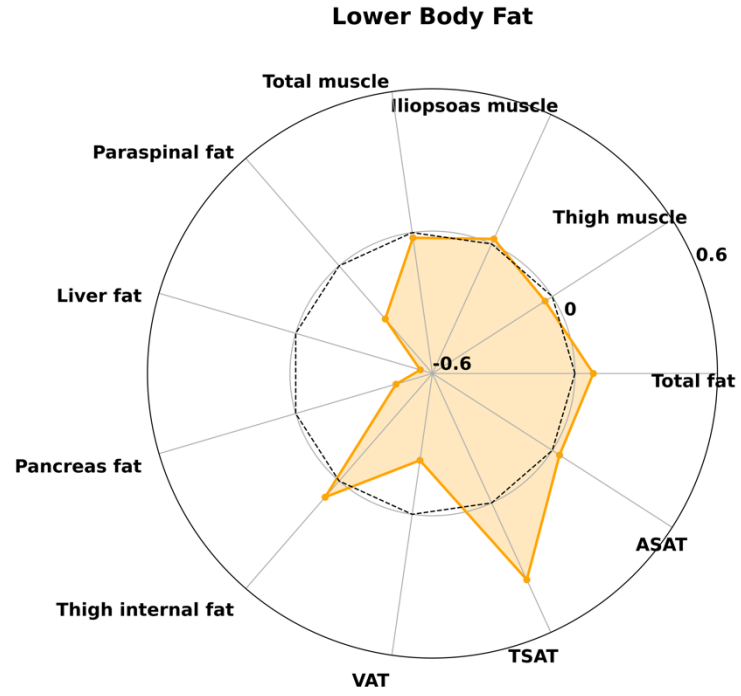

Figure 2 A

Diabetes
General Obesity

Individual with low score

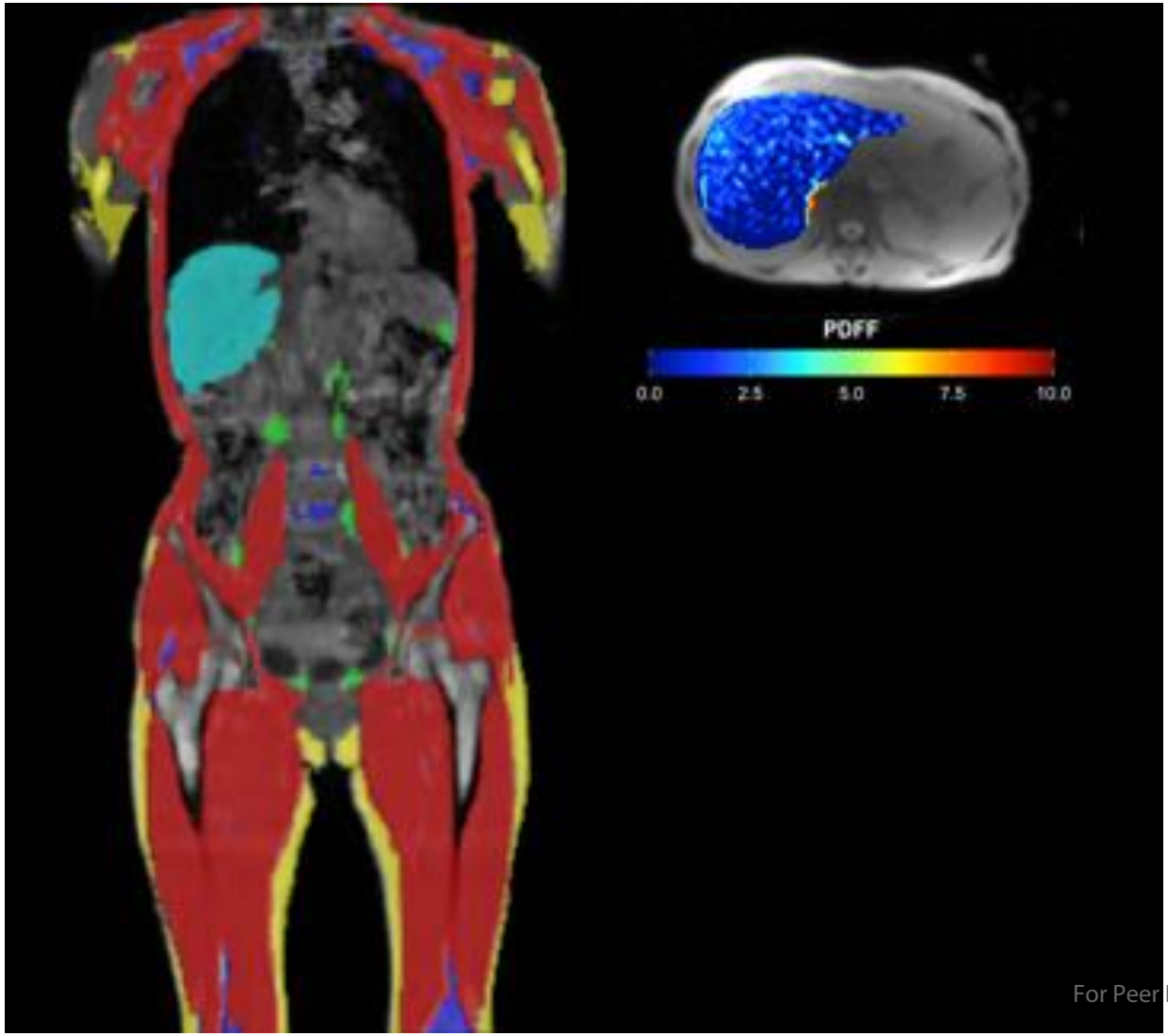

Individual with high score

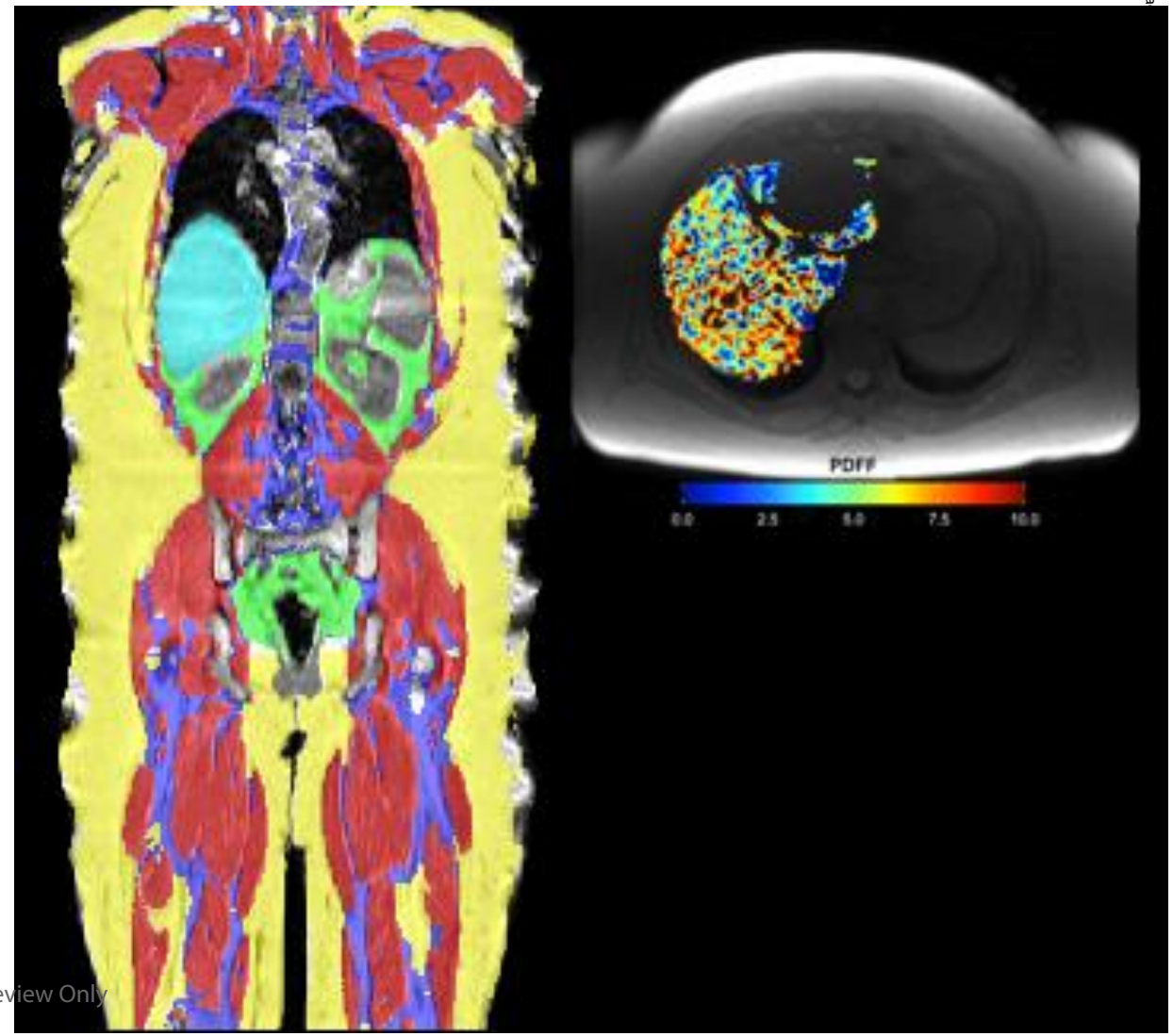

Muscle-Dominant

Individual with low score

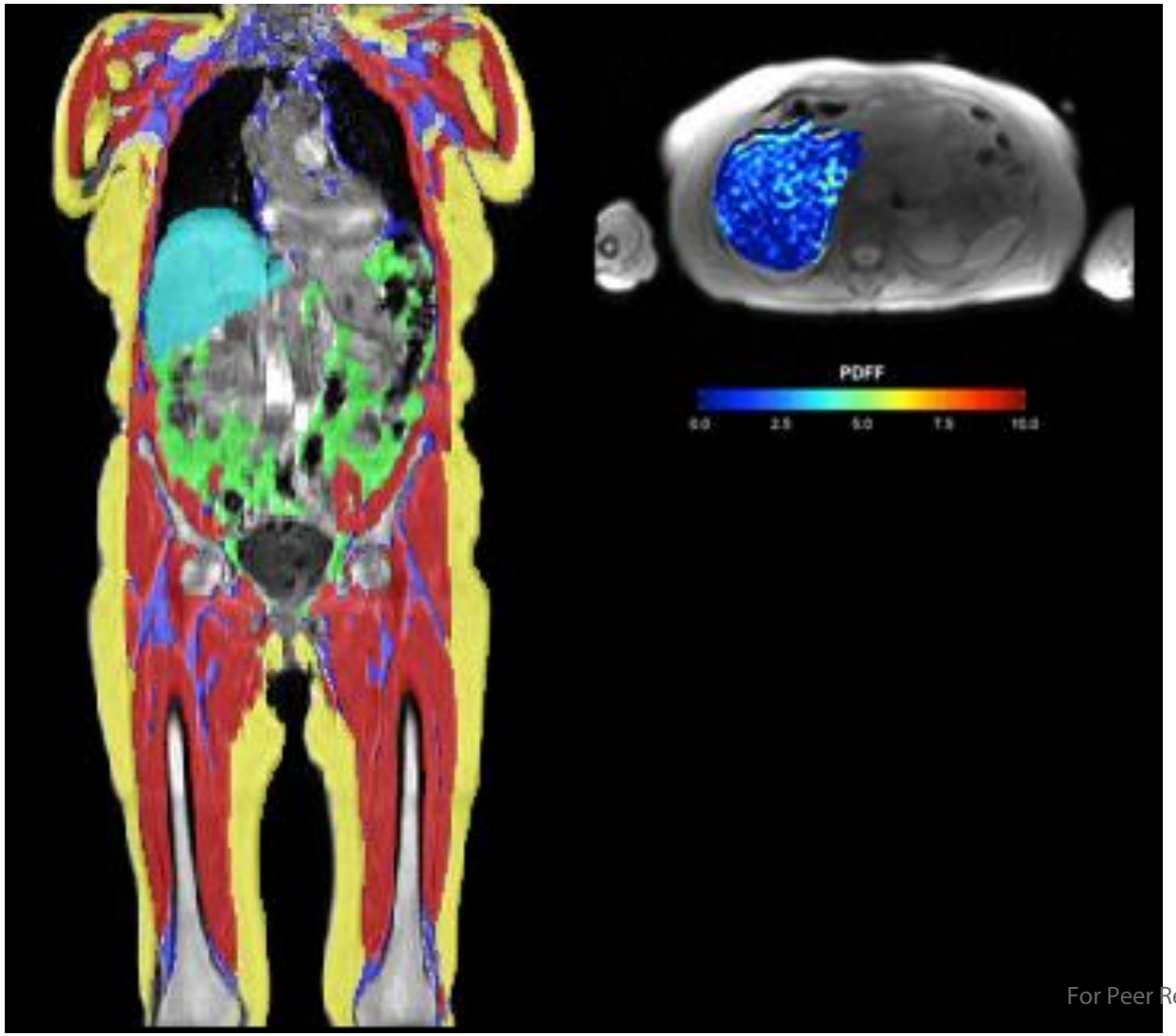

Individual with high score

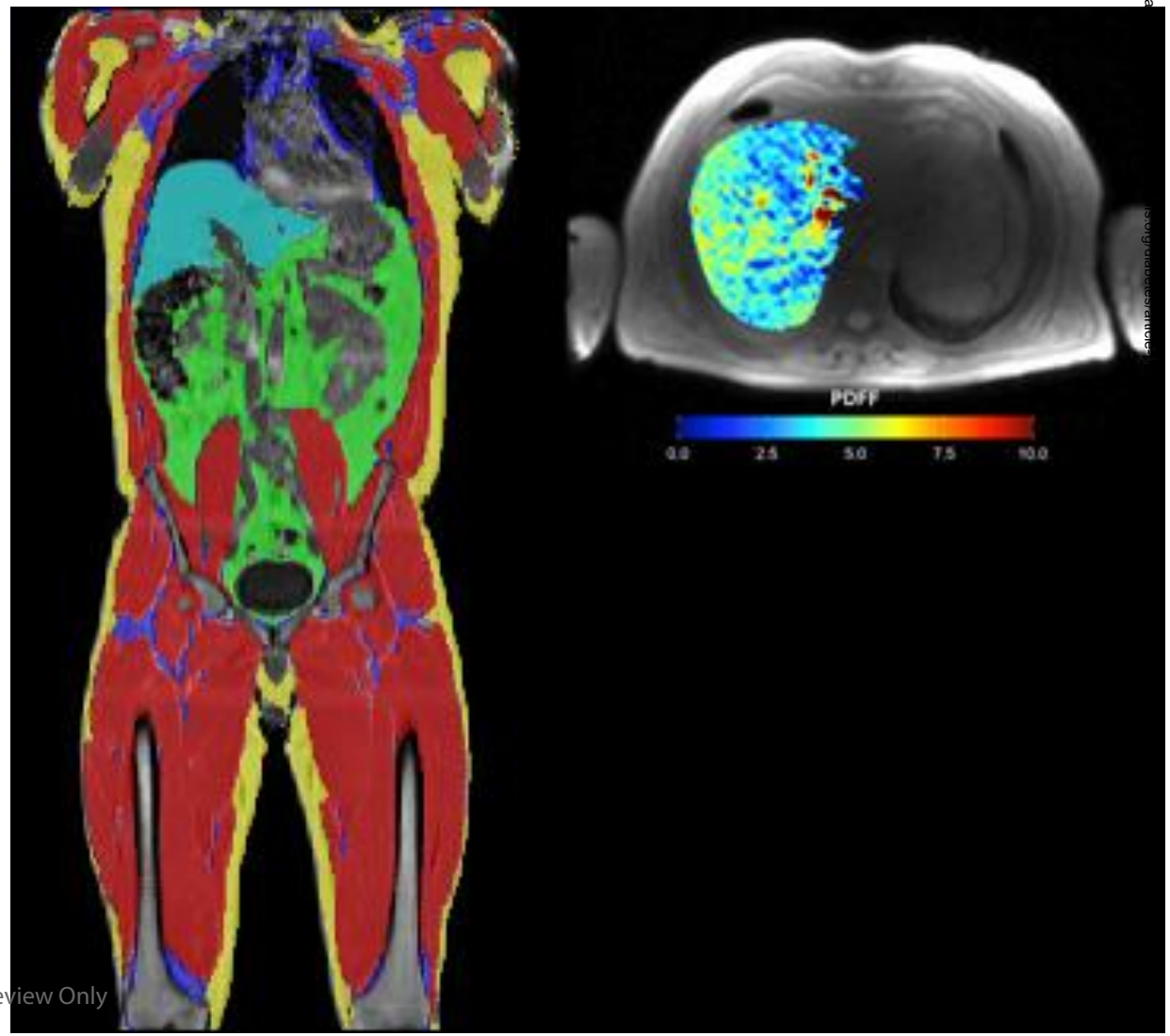

Figure 2 C

Diabetes
Peripheral Fat

Individual with low score

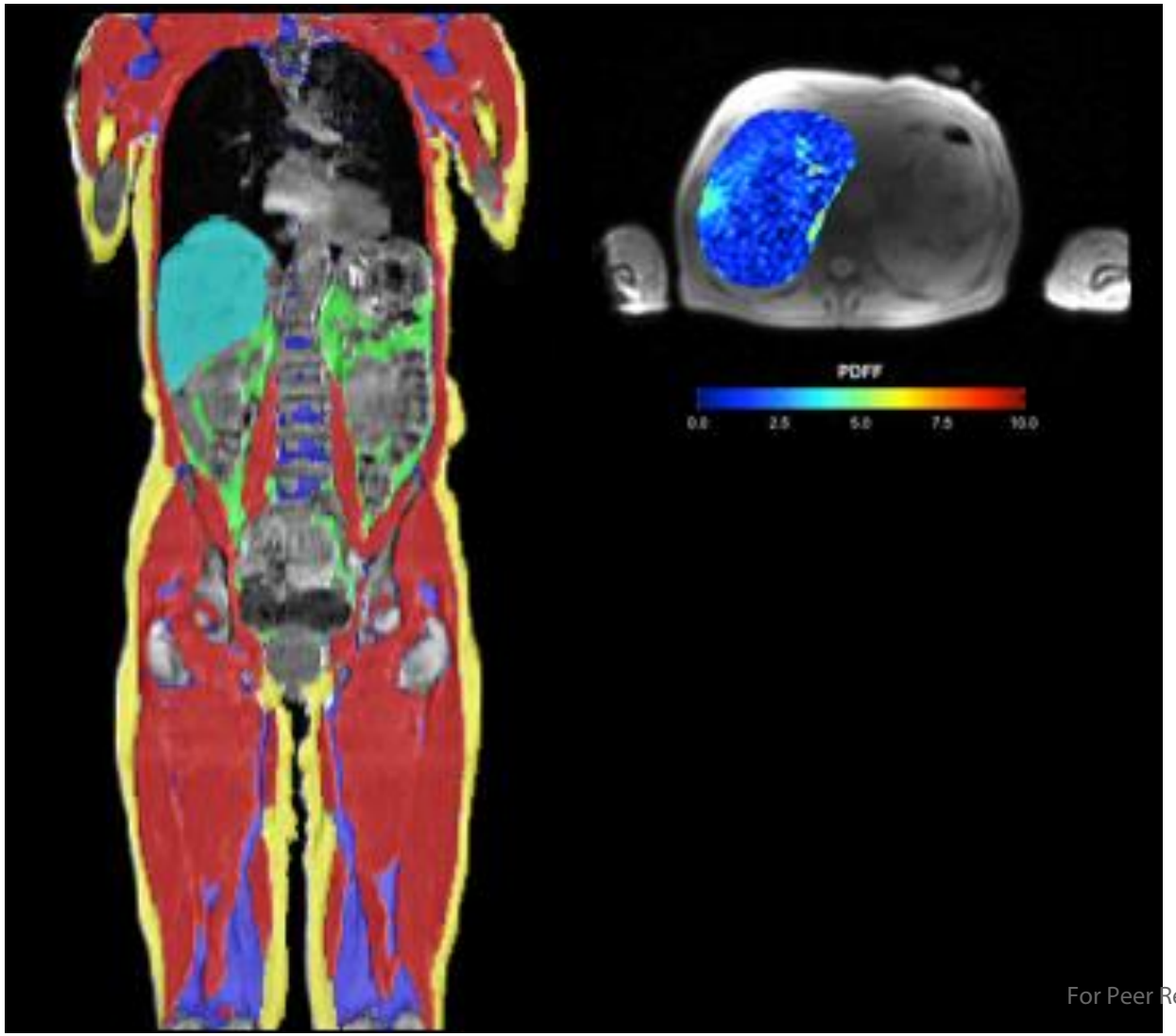

Individual with high score

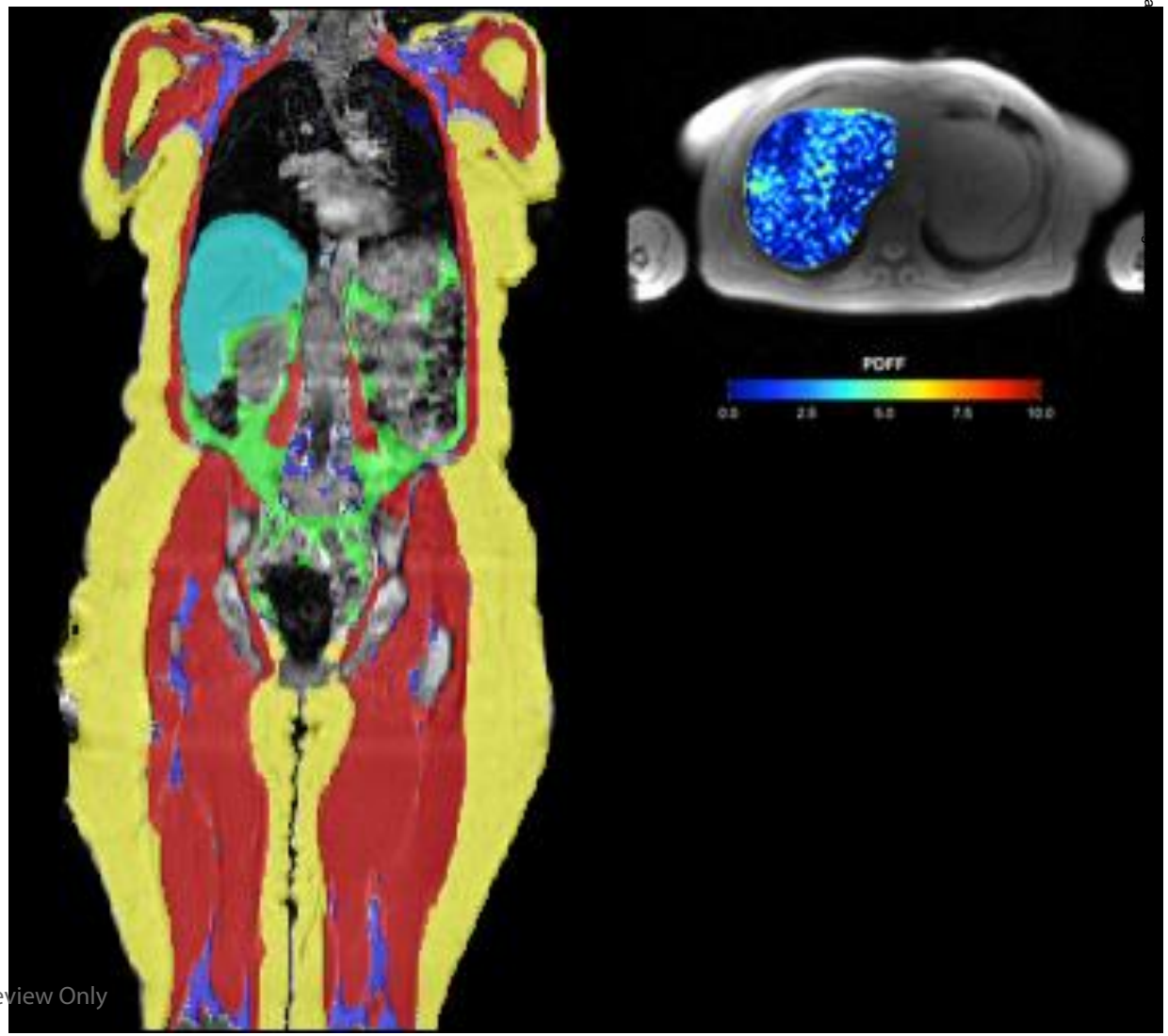

Lower Body Fat

Individual with low score

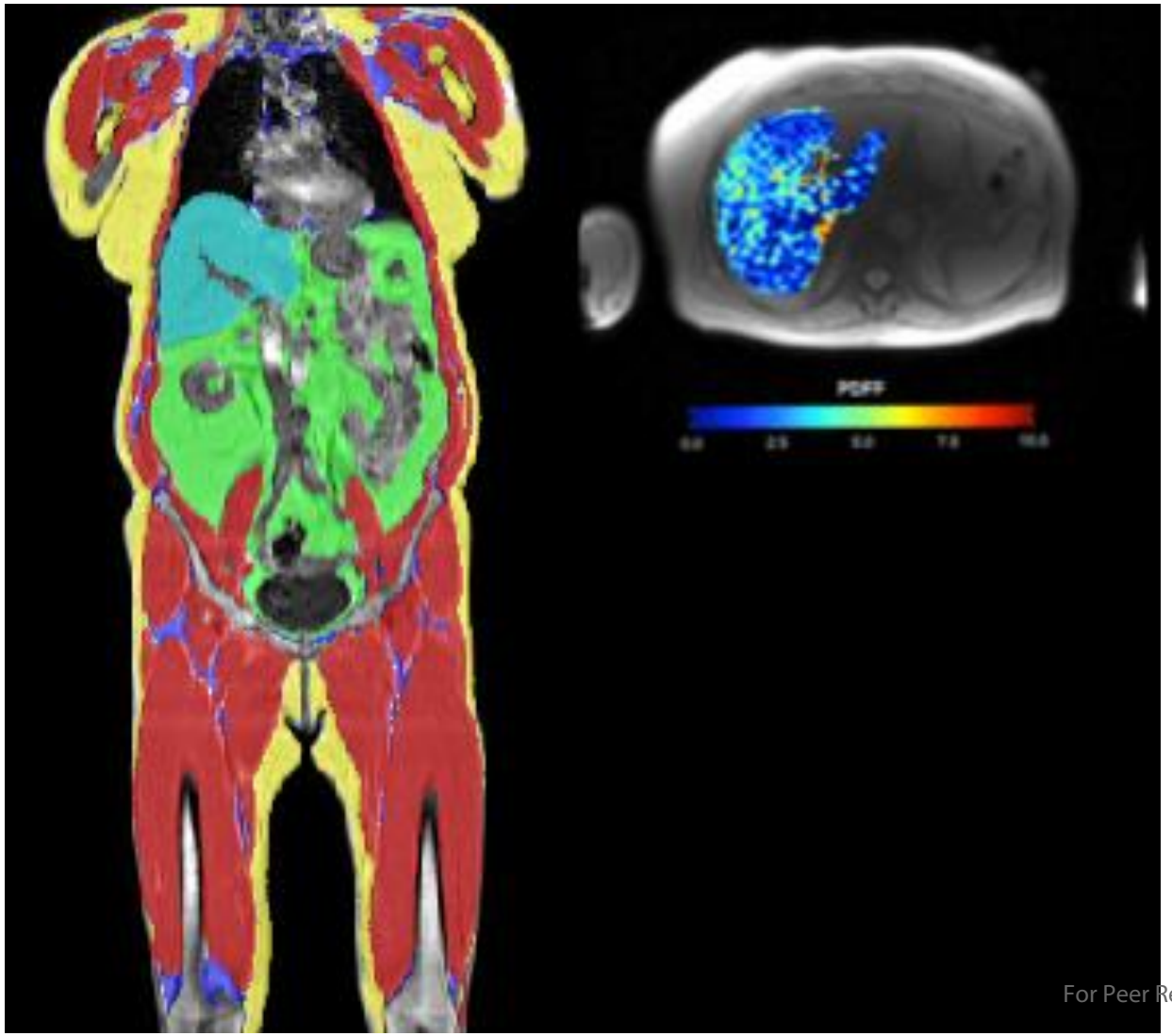

Individual with high score

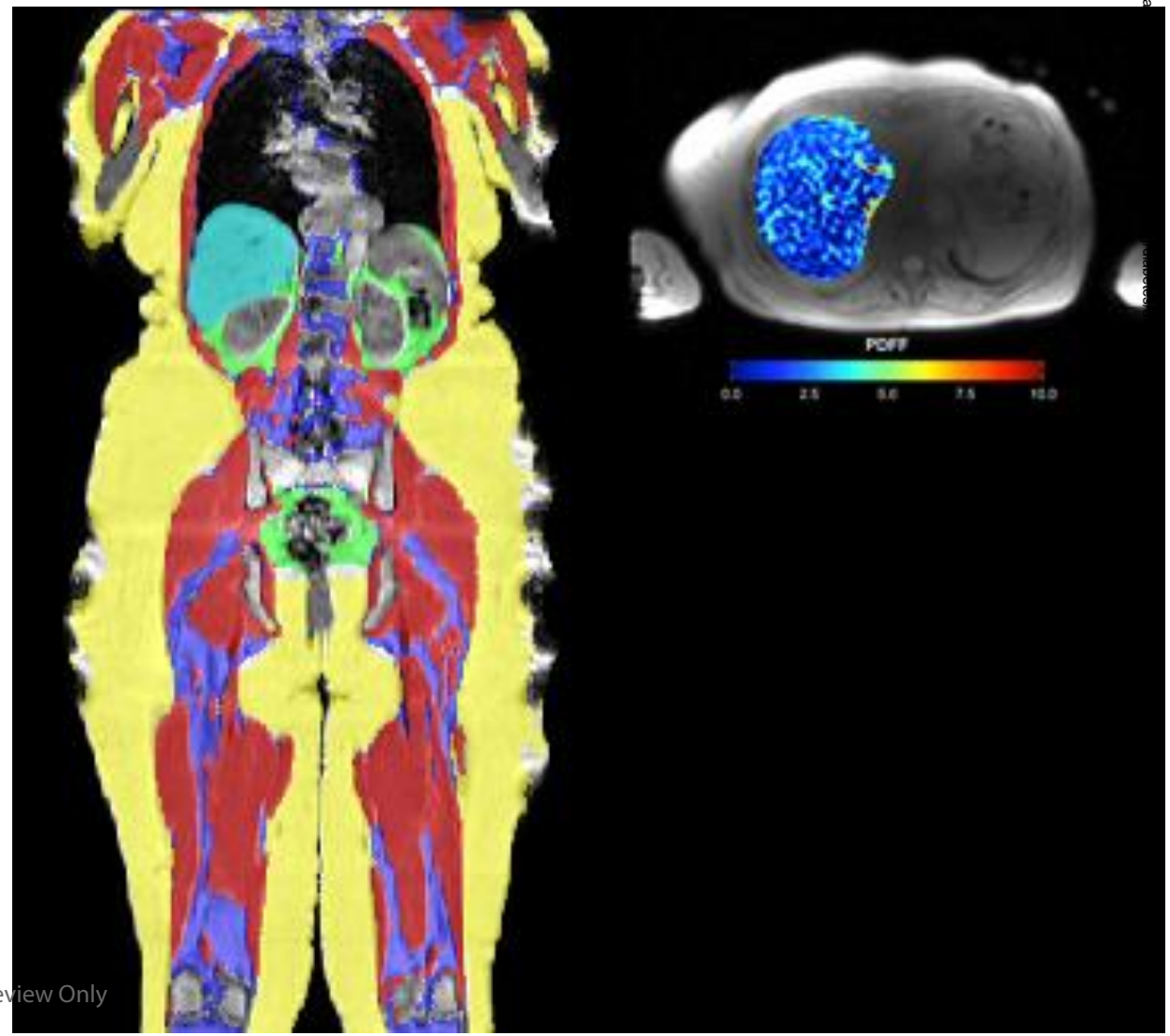

Figure 3

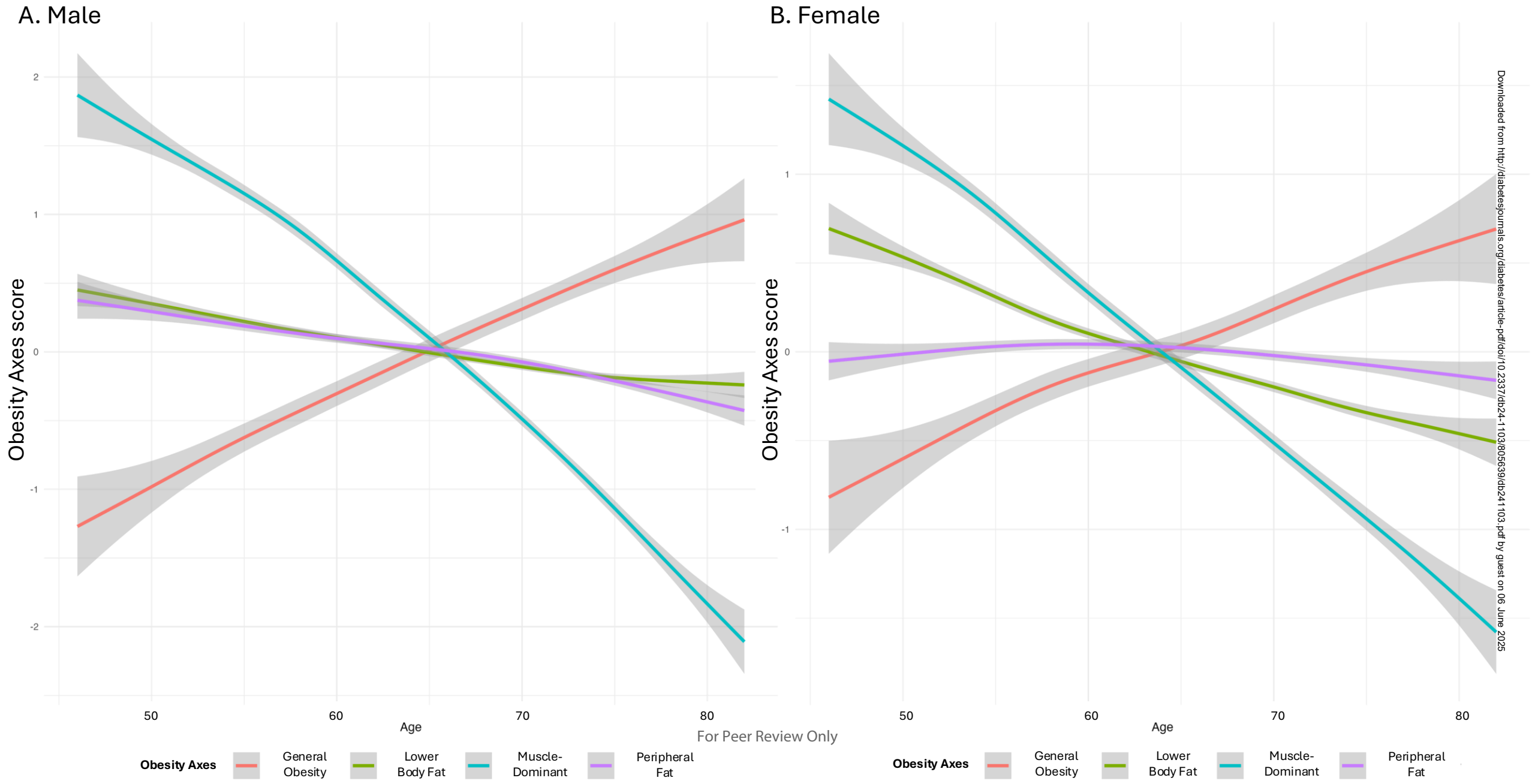

Figure 4

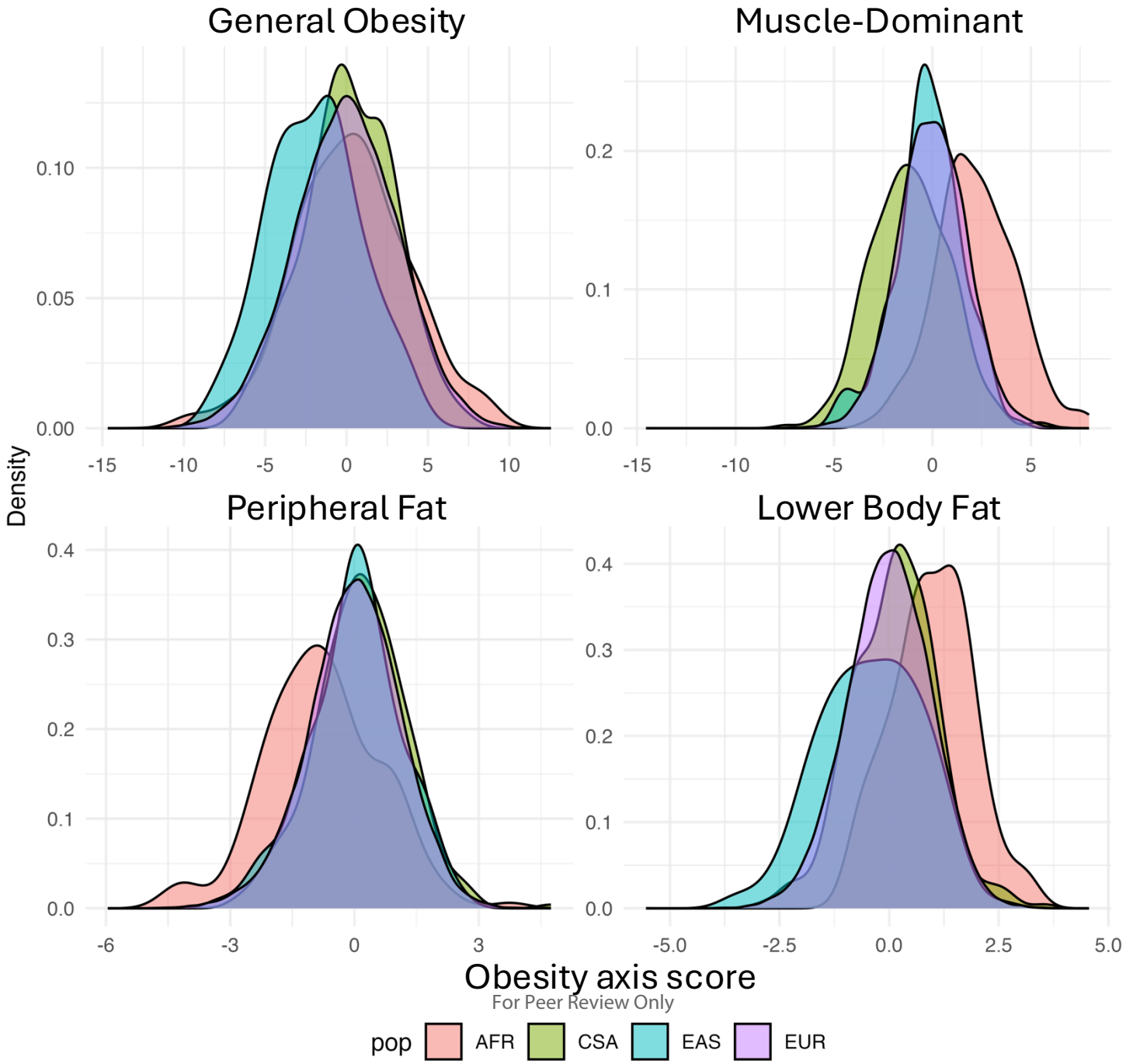

Figure 5

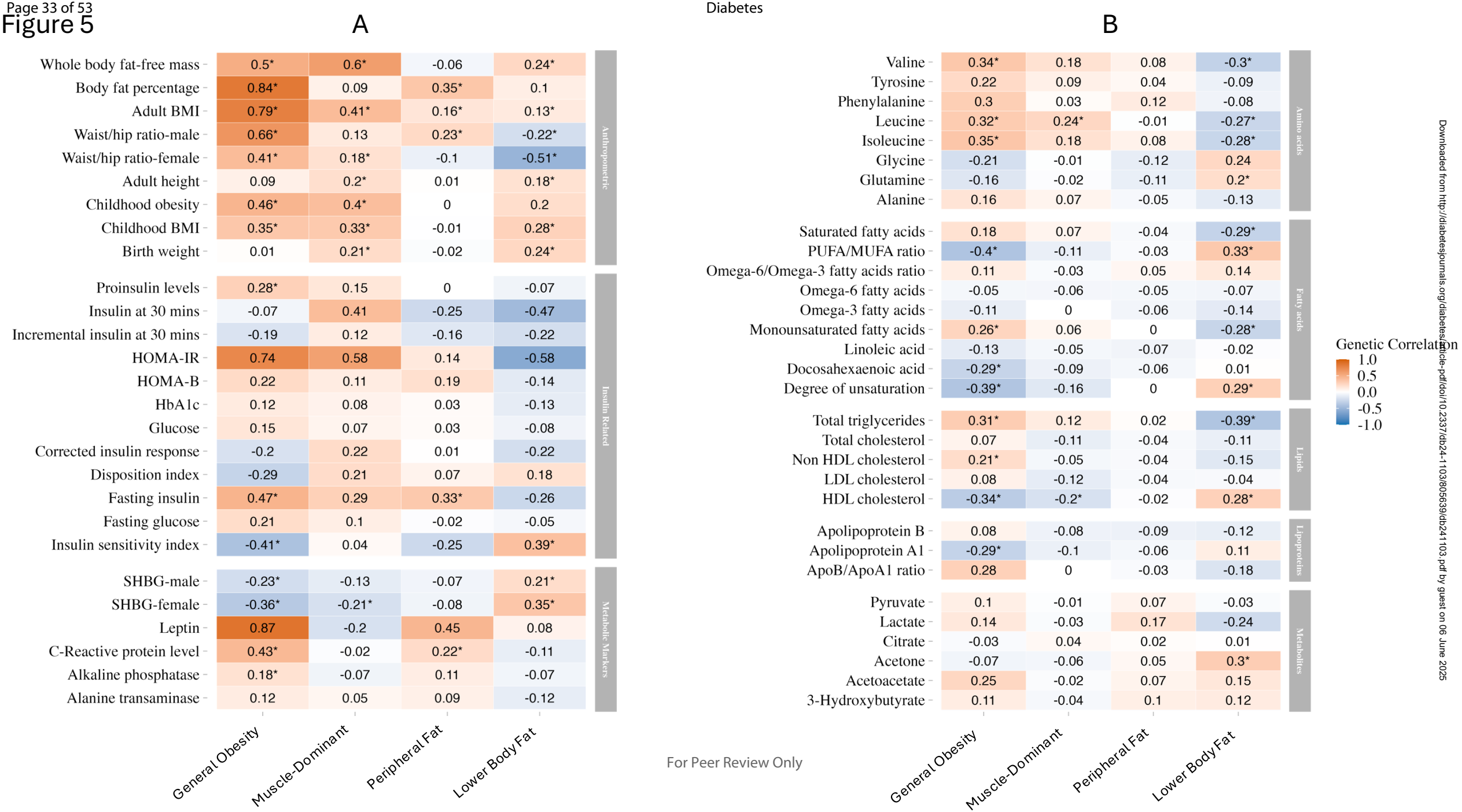

Figure 5

C

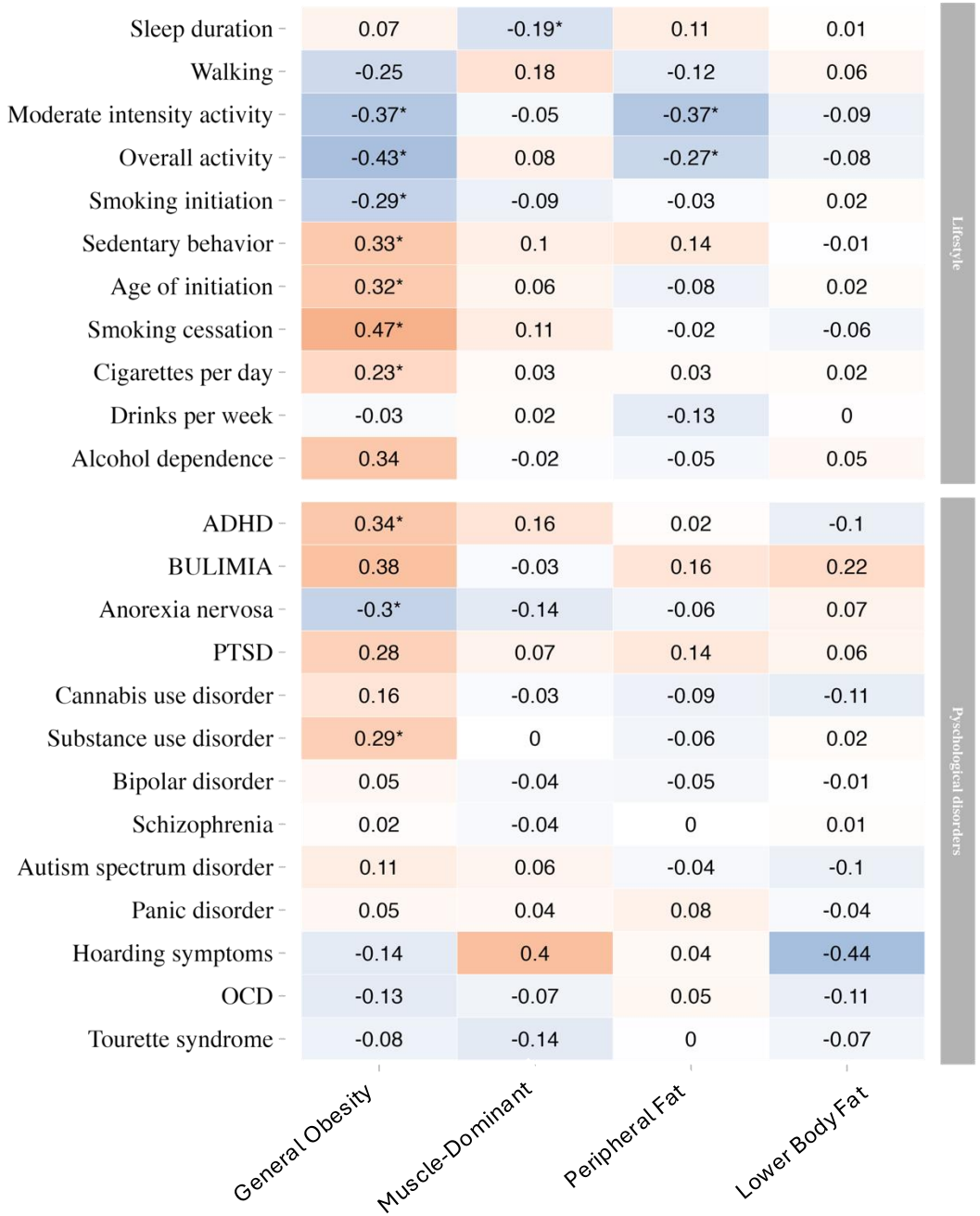

D

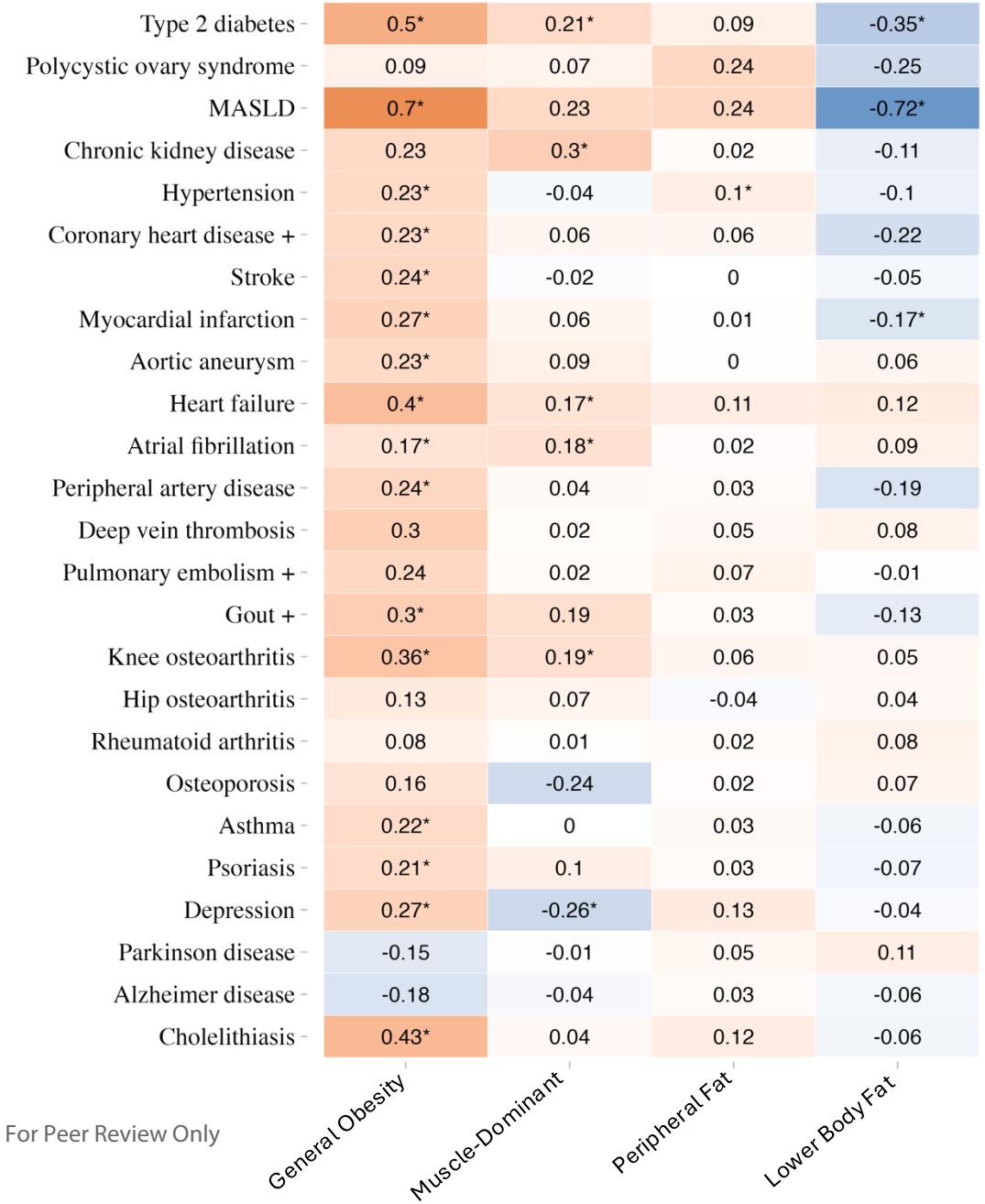

Figure 6

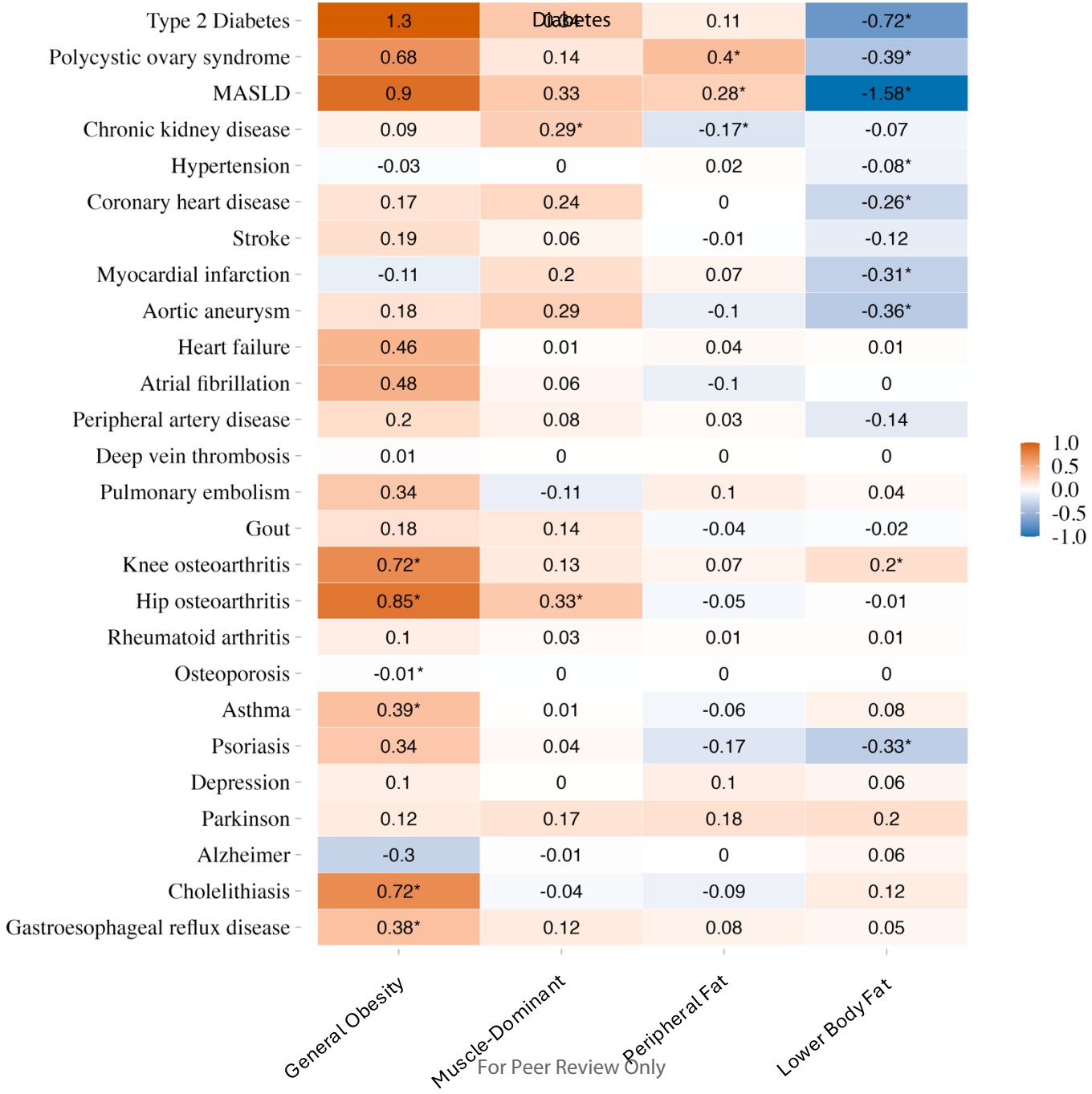

Supplementary Table 1: Summary of data used in the study. This table provides an overview of the 24 image-derived phenotypes (IDPs) included in the study. These measures were derived from MRI imaging and represent various fat distribution and muscle characteristics across different anatomical regions. IMAT: intermuscular adipose tissue; PDFF: proton density fat fraction.

	Male	**Female**	**Combined**
No of Participants	16169	16953	33122
Age (Years) Mean±SD	65.37±7.72	63.98±7.46	64.66±7.62
BMI (Mean±SD)	26.82±3.73	26.02±4.63	26.41±4.23
Alcohol Intake Frequency (Daily) (n)	3285	2257	5542
Alcohol Intake Frequency (3-4x/Week) (n)	5161	4309	9470
Alcohol Intake Frequency (1-2x/Week) (n)	4185	4553	8738
Alcohol Intake Frequency (1-3x/Month) (n)	1538	2262	3800
Alcohol Intake Frequency (Special Occasions) (n)	1051	2192	3243
Alcohol Intake Frequency (Never) (n)	941	1374	2315
Alcohol Intake Frequency (No response) (n)	8	6	14
Current Smoker (n)	9014	8295	17309
Never Smoker (n)	7008	8514	15522
Former Smoker (n)	29	0	29
Type 2 Diabetes (% Case)	5.57	2.24	3.86
Hypertension (% Case)	38.43	25.03	31.57
Stroke (% Case)	3.30	3.27	3.28
Myocardial infarction (% Case)	4.95	1.03	2.94
Aortic aneurysm (% Case)	0.67	0.14	0.40
Heart failure (% Case)	1.82	0.62	1.20
Atrial fibrillation (% Case)	6.55	2.77	4.61
Pulmonary embolism (% Case)	1.48	0.99	1.23
Gout (% Case)	6.39	0.44	3.35
Osteoarthritis (% Case)	7.69	7.62	7.65
Rheumatoid arthritis (% Case)	2.87	2.80	2.83
Osteoporosis (% Case)	1.13	6.13	3.69
Asthma (% Case)	13.28	14.16	13.73
Psoriasis (% Case)	4.00	3.09	3.54
Depression (% Case)	8.08	11.19	9.67
Parkinson's disease (% Case)	0.38	0.19	0.28
Alzheimer's disease (% Case)	0.06	0.05	0.06
Chronic Ischaemic Heart Disease (% Case)	9.51	2.50	5.92
Total Fat (Mean±SD) L	22.73 ± 8.16	26.57 ± 9.28	24.69±8.96
Subcutaneous fat (Mean±SD) L	14.71 ± 5.49	21.52 ± 7.52	18.20±7.43

Abdominal subcutaneous fat (Mean±SD) L	6.94 ± 3.14	9.84 ± 4.30	8.42±4.05
Internal fat (Mean±SD) L	2.88 ± 1.15	2.22 ± 0.83	2.54±1.05
Thigh subcutaneous fat (Mean±SD) L	5.82 ± 2.08	8.97 ± 2.96	7.43±3.01
Thigh IMAT (Mean±SD) L	0.84 ± 0.36	0.71 ± 0.29	0.77±0.33
Mid-thigh IMAT (Mean±SD) L	0.05 ± 0.05	0.05 ± 0.04	0.05±0.04
Mid-thigh subcutaneous fat (Mean±SD) L	1.24 ± 0.45	2.06 ± 0.76	1.66±0.75
Index thigh IMAT (Mean±SD) L/m^2	0.27 ± 0.12	0.27 ± 0.11	0.27±0.11
Index mid-thigh IMAT (Mean±SD) L/m^2	0.02 ± 0.02	0.02 ± 0.01	0.02±0.01
Visceral fat (Mean±SD) L	5.14 ± 2.31	2.83 ± 1.55	3.96±2.27
PDFF liver (Mean±SD) %	5.48 ± 5.00	4.18 ± 4.49	4.82±4.79
PDFF paraspinal (Mean±SD) %	7.01 ± 3.72	8.03 ± 4.17	7.53±3.99
PDFF pancreas (Mean±SD) %	12.92 ± 8.76	8.53 ± 6.85	10.67±8.15
Total muscle (Mean±SD) L	21.72 ± 2.92	14.03 ± 1.94	17.79±4.57
Thigh muscle (Mean±SD) L	10.30 ± 1.48	6.68 ± 1.00	8.45±2.21
Mid-thigh muscle (Mean±SD) L	2.71 ± 0.40	1.87 ± 0.28	2.28±0.54
Iliopsas muscle (Mean±SD) L	0.78 ± 0.12	0.51 ± 0.08	0.64±0.17
Index iliopsas muscle (Mean±SD) L/m^2	0.25 ± 0.03	0.19 ± 0.02	0.22±0.04
Index thigh muscle (Mean±SD) L/m^2	3.32 ± 0.40	2.52 ± 0.31	2.91±0.54
Index tmid-thighmuscle (Mean±SD) L/m^2	0.88 ± 0.12	0.71 ± 0.10	0.79±0.14
Index total muscle (Mean±SD) L/m^2	7.00 ± 0.79	5.29 ± 0.61	6.13±1.11
Ratio thigh internal fat to thigh muscle (Mean±SD)	0.08 ± 0.03	0.10 ± 0.03	0.09±0.03
Ratio mid-thigh internal fat to mid-thigh muscle (Mean±SD)	0.02 ± 0.02	0.02 ± 0.02	0.02±0.02

Supplementary Table 2: Traits used in the genetic correlation study of obesity axes and Mendelian randomization. These traits span anthropometric measures, metabolic biomarkers, lifestyle behaviors, psychological conditions, and disease outcomes.

Trait	PubMed ID	Sample size Case/control Pubgwas	Phenocode Pubgwas	Phenocode FinnGen	Case/control FinnGen	Author Pubgwas	Data Freeze FinnGen	Include UKBB Data
ADHD	36702997	186,843	NA	NA	NA	Demontis 2023		NO
Panic disorder	31712720	7992	NA	NA	NA	Forstner 2021		NO
Autism spectrum disorder	30804558	27,969	NA	NA	NA	Grove 2019		NO
Bipolar disorder	34002096	371,549	NA	NA	NA	Mullins 2021		YES
Anorexia nervosa	31308545	55,525	NA	NA	NA	Watson 2019		YES
Tourette syndrome	30818990	9,488	NA	NA	NA	Yu 2019		NO
OCD	28761083	7037	NA	NA	NA	Posthuma 2018		NO
Hoarding symptoms	36379924	NA	NA	NA	NA	Strom 2022		NO
PTSD	31594949	170,000	NA	NA	NA	Nievergelt 2019		YES
Schizophrenia	35396580	243,649	NA	NA	NA	Trubetskoy 2022		NO
Substance use disorder	37250466	NA	NA	NA	NA	Hatoum 2023		NO

Opioid dependence	32099098	NA	NA	NA	NA	Polimanti 2020		NO
Cannabis use disorder	33096046	357,219	NA	NA	NA	Johnson 2020		NO
Alcohol use	30336701	NA	NA	NA	NA	Sanchez-Roige 2019		YES
Alcohol dependence	30482948	34,999	NA	NA	NA	Walters 2018		NO
Cytokines and growth factors	27989323, 33491305	8,293	NA	NA	NA	Ahola-Olli AV(2017), Kalaoja(2021)		NO
Metabolites	35692035	114000	met-d-*	NA	NA	Borges CM(2022)		YES
Childhood BMI	33045005	39,620	NA	NA	NA	Vogelezang S (2020)		NO
Childhood Obesity	31504550	24160	ebi-a-GCST90002409	NA	NA	Bradfield JP(2019)		NO
HbA1c	34059833	281416	ebi-a-GCST90002244	NA	NA	Chen J(2021)		NO
Adiponectin	22479202	45891	ieu-a-1	NA	NA	Dastani Z (2012)		NO
HOMA-B, HOMA-IR	20081858	46186	ieu-b-117/118	NA	NA	Dupius J(2010)		NO
HDL, LDL and non-HDL cholesterol, Total cholesterol, Triglycerides	34887591, 36575460, 35931049	1320000	ieu-a-1002	NA	NA	Graham SE(2021); Kanoni S(2022); Ramdas S(2022)		YES
Leptin	26833098	32161	NA	NA	NA	Kilpel€ainen TO(2016)		NO
Fasting glucose, Fasting insulin	33558525	140595, 98210	NA	NA	NA	Lagou V(2021)		NO
Disposition index, corrected insulin response, insulin at 30 mins, incremental insulin at 30 mins	24699409	5318	NA	NA	NA	Prokopenko I(2014)		NO
Adult BMI, waist-to-hip ratio (combined), waist-to-hip ratio (combined)	30239722	806834, 379501, 315284	NA	NA	NA	Pulit SL(2019)		YES
Adult height	36224396	4080687	NA	NA	NA	Yengo L(2022)		YES
Proinsulin Levels	36693378	45861	NA	NA	NA	Broadway A. K(2023)		NO
Insulin sensitivity index	37291194	55,535 and 55,172 (w/o diabetes)	NA	NA	NA	Williamson(2023)		NO
Birth weight	31043758	298142	NA	NA	NA	Warrington NM(2019)		YES
Body fat percentage	NA	454633	NA	NA	NA	Elsworth B(2018)		NO
C-Reactive protein	30388399	204402	NA	NA	NA	Ligthart S(2018)		NO
Whole body fat-free mass	NA	454850	NA	NA	NA	Elsworth B(2018)		YES
Sex hormone-binding globulin (female)	NA	214989	NA	NA	NA	Richmond R(2020)		YES
Sex hormone-binding globulin (male)	NA	185221	NA	NA	NA	Richmond R(2020)		YES
Liver enzymes: ALT, ALP,GGT	33972514	437438, 437267, 437194	NA	NA	NA	Pazoki R (2021)		YES

Type 2 diabetes	35551307	80154/853816	NA	T2D	65085/335112	Mahajan A (2022)	DF10	
Polycystic ovary syndrome	34791234	797/140558	ebi-a-GCST90044902	E4_PCOS	2544/408430	Tyrmi JS	DF10	
MASLD	34841290	8434/770180	ebi-a-GCST90091033	NAFLD	2568/409613	Ghodsian N(2021)	DF10	
Chronic kidney disease	31152163	41395/439303	Wuttke, 2019	N14_CHRONKIDNEYDIS	10039/396706	Wuttke (2019)	DF10	
Hypertension	33959723	129909/354689	ebi-a-GCST90038604	I9_HYPTENS	122996/289117	Dönertaş et al. (2021)	DF10	
Coronary heart disease	26343387	22233/64762	ebi-a-GCST003116	I9_ATHSCLE	16243/381977	Nickpay 2015	DF10	
Stroke	26343387	34217/406111	ebi-a-GCST006908	I9_STR	27497/371723	Malik R. 2018	DF10	
Myocardial infarction	33532862	14825/2680	ebi-a-GCST011364	I9_MI_STRICT	26060/343079	Hartiala JA et al. 2021	DF10	
Aortic aneurysm	34594039	3230/475964	ebi-a-GCST90018783	I9_AORTANEUR	8125/381977	Sakaue S(2021)	DF10	
Heart failure	31919418	47309/930014	ebi-a-GCST009541	I9_HEARTFAIL	29672/382509	Shah et al. 2020	DF10	
Atrial fibrillation	30061737	60620/970216	ebi-a-GCST006414	I9_AF	50743/210652	Nielsen JB et al. 2018	DF10	
Peripheral artery disease	34594039	7114/475964	ebi-a-GCST90018890	I9_PAD	11924/288638	Sakaue S(2021)	DF7	
Deep vein thrombosis	33959723	9529/475069	ebi-a-GCST90038615	I9_PHLETHROMBDVTLOW	6501/357111	Dönertaş et al. (2021)	DF10	
Pulmonary embolism	34017140	407,746	ebi-a-GCST90013937	I9_PULMEMB	10046/401128	Mbatchou J(2021)	DF10	
Gout	23263486	2115/69374	ieu-a-1054	M13_GOUT	9568/262844	Kottgen(2013)	DF10	
Knee osteoarthritis	30664745	24955/378169	ebi-a-GCST007090	M13_ARTHROSIS_KNEE	48836/262844	Tachmazidou(2019)	DF10	
Hip osteoarthritis	30664745	15704/378169	ebi-a-GCST007091	M13_ARTHROSIS_COX	80598/262844	Tachmazidou(2019)	DF10	
Rheumatoid arthritis	33310728	14361/43923	ebi-a-GCST90013534	M13_RHEUMA	13621/262844	Ha E (2020)	DF10	
Osteoporosis	33959723	7751/476847	ebi-a-GCST90038656	M13_OSTEOPOROSIS	8017/391037	Dönertaş et al. (2021)	DF10	
Asthma	34103634	56167/352255	ebi-a-GCST90014325	J10_ASTHMA_MAIN_EXMORE	37760/219734	Valette K(2021)	DF10	
Psoriasis	34927100	15967/ 28169	ebi-a-GCST90019017	L12_PSORIASIS	10312/397564	Stuart PE(2021)	DF10	
Depression	34594039	13559/435855	ebi-a-GCST90018833	F5_DEPRESSIO	47696/359290	Sakaue S(2021)	DF10	
Parkinson's disease	31701892	33674/449056	ieu-b-7	G6_PARKINSON	4681/407500	Nalls MA(2019)	DF10	
Alzheimer's disease	35379992	39106/46828	ebi-a-GCST90027158	G6_ALZHEIMER	10520/401661	Bellenguez C(2022)	DF10	

Cholelithiasis	34594039	26122/461431	ebi-a-GCST90018819	K11_CHOLELITH	40191/361641	Sakaue S(2021)	DF10	
Gastroesophageal reflux disease	34187846	129080/473524	ebi-a-GCST90000514	K11_REFLUX	28859/350064	Ong Js (2021)	DF10	

Supplementary Table 3: Contributions of MRI-derived phenotypes to obesity axes. This table provides a comprehensive overview of all 24 MRI-derived phenotypes used in the principal component (PC) analysis, along with their corresponding loadings on each obesity axis.

PCs	PC1	PC2	PC3	PC4	PC1	PC2	PC3	PC4
Sex	Male	Male	Male	Male	Female	Female	Female	Female
Abdominal subcutaneous fat	0.23	0.10	0.35	0.04	0.27	0.09	0.31	0.04
Iliopsoas muscle	0.01	0.29	-0.03	0.02	0.03	0.27	-0.08	0.10
Internal fat	0.28	-0.07	-0.14	-0.10	0.26	-0.10	-0.16	-0.07
Total muscle	0.02	0.30	-0.07	0.04	0.05	0.29	-0.13	0.07
Visceral fat	0.24	0.08	0.14	-0.34	0.22	0.03	0.13	-0.23
Mid-thigh IMAT	0.31	-0.04	-0.22	0.09	0.27	-0.10	-0.25	0.06
Index mid-thigh muscle	0.04	0.33	-0.09	0.03	0.07	0.33	-0.15	0.01
Mid-thigh subcutaneous fat	0.18	0.11	0.34	0.30	0.18	0.08	0.31	0.37
PDFF erosion median pancreas	0.16	-0.02	0.09	-0.60	0.19	-0.03	0.16	-0.44
PDFF erosion median ideal liver	0.15	0.12	0.08	-0.41	0.21	0.10	0.16	-0.55
PDFF erosion median ideal paraspinal	0.21	-0.09	-0.03	-0.30	0.22	-0.06	0.04	-0.30
Ratio mid-thigh internal fat to mid-thigh muscle	0.29	-0.14	-0.19	0.08	0.26	-0.20	-0.22	0.06
Index iliopsoas muscle	0.02	0.32	-0.10	-0.02	0.04	0.29	-0.07	0.02
Index total muscle	0.03	0.33	-0.16	0.00	0.07	0.33	-0.14	-0.02
Subcutaneous fat	0.23	0.08	0.35	0.12	0.25	0.08	0.32	0.15
Total fat	0.28	0.08	0.27	-0.03	0.29	0.07	0.29	0.08
Index thigh IMAT	0.29	-0.08	-0.24	0.13	0.28	-0.11	-0.22	0.09
Index thigh muscle	0.03	0.34	-0.17	0.00	0.06	0.34	-0.16	-0.04
Index mid-thigh IMAT	0.30	-0.06	-0.23	0.08	0.27	-0.11	-0.25	0.04
Index mid-thigh muscle	0.05	0.37	-0.18	-0.02	0.08	0.35	-0.15	-0.09
Thigh IMAT	0.29	-0.05	-0.20	0.15	0.28	-0.09	-0.23	0.13
Thigh muscle	0.02	0.31	-0.08	0.04	0.05	0.30	-0.14	0.05
Thigh subcutaneous fat	0.21	0.08	0.36	0.27	0.20	0.07	0.30	0.36
Ratio thigh internal fat to thigh muscle	0.26	-0.22	-0.16	0.12	0.24	-0.25	-0.15	0.10

Supplementary Table 4: BMI distributions in the top and bottom 10% of each obesity axis as defined by our principal component analysis. Min: minimum; max: maximum; sd: standard deviation.

Axis	Class	Sex	BMI min	BMI max	BMI median	BMI mean	BMI sd	BMI>30

General Obesity	Top	Female	22.2	55.2	34.1	34.5	4.6	1400
General Obesity	Bottom	Female	15.3	26.9	20.6	20.6	1.7	0
Muscle-Dominant	Top	Female	16.3	55.2	27.7	28.8	5.8	614
Muscle-Dominant	Bottom	Female	15.3	44.9	23.0	23.4	3.5	56
Peripheral Fat	Top	Female	16.7	55.2	27.1	28.0	5.3	500
Peripheral Fat	Bottom	Female	16.1	42.3	23.6	24.3	3.8	140
Lower Body Fat	Top	Female	18.2	52.1	25.7	26.8	5.1	334
Lower Body Fat	Bottom	Female	15.7	41.6	25.5	25.8	4.1	243
General Obesity	Top	Male	22.9	50.5	32.6	33.0	3.7	1233
General Obesity	Bottom	Male	16.5	31.3	22.4	22.3	1.8	1
Muscle-Dominant	Top	Male	20.6	50.5	29.7	30.1	4.0	736
Muscle-Dominant	Bottom	Male	16.5	41.8	24.0	24.3	3.1	69
Peripheral Fat	Top	Male	18.0	45.4	27.6	28.2	4.4	460
Peripheral Fat	Bottom	Male	17.6	44.5	26.0	26.3	3.5	224
Lower Body Fat	Top	Male	17.6	44.9	26.0	26.9	4.3	319
Lower Body Fat	Bottom	Male	18.6	42.7	26.3	26.5	3.0	187

Supplementary Table 5: Comparison of obesity axes scores across ancestry groups. This table presents the mean and standard deviation (SD) of obesity axes scores for individuals of African ancestry (AFR; N=146), Central/South Asian ancestry (CSA; N=320), East Asian ancestry (EAS; N=152), and European ancestry (EUR; N=29,179).

Obesity axes	Mean/SD in EUR	Mean/SD in AFR	Mean/SD in CSA	Mean/SD in EAS	p-value (EUR vs AFR)	p-value (EUR vs CSA)	p-value (EUR vs EAS)
General Obesity	0 ± 3.18	0.33 ± 3.5	0.21 ± 2.79	-1.97 ± 2.85	0.2576	0.18442	<0.00001
Muscle-Dominant	-0.01 ± 1.77	2.21 ± 2	-1.11 ± 1.99	-0.21 ± 1.69	<0.00001	<0.00001	0.14081
Peripheral Fat	0 ± 1.13	-0.79 ± 1.39	0.16 ± 1.09	0.01 ± 1.1	<0.00001	0.01235	0.94422
Lower Body Fat	-0.01 ± 0.96	0.98 ± 0.92	0.11 ± 0.97	-0.41 ± 1.16	<0.00001	0.03395	0.00004

Supplementary Table 6: Genetic loci associated with obesity axes and consistency across sexes. This table summarises the genetic loci contributing to the obesity axes, highlighting the lack of evidence for sex-specific associations. The loci were consistent between males (M) and females (F), as shown by the heterogeneity p-value (HetPVal).

Axis	A1	A2	rsID	Effect Size (F)	Effect Size (F)	Effect Size (F)	Number (F)	Effect Size (M)	Effect Size (M)	Effect Size (M)	Number (M)	HetPVal
General Obesity	t	c	rs62033405	0.05	0.01	1.5e-05	13034	0.06	0.01	7.4e-07	12603	0.6207
General Obesity	t	c	rs33823	0.06	0.01	7.1e-06	13034	0.05	0.01	2.7e-05	12603	0.8712
Muscle-Dominant	t	g	rs7515497	-0.05	0.01	7.4e-06	13034	-0.04	0.01	0.0007	12603	0.4658
Muscle-Dominant	a	g	rs3850625	-0.08	0.02	6.9e-06	13034	-0.05	0.02	0.001	12603	0.3953
Muscle-Dominant	a	c	rs2138157	-0.04	0.01	0.00012	13034	-0.05	0.01	2.8e-05	12603	0.7706

Muscle-Dominant	t	c	rs12632536	-0.05	0.01	4.4e-05	13034	-0.05	0.01	2.2e-05	12603	0.8711
Muscle-Dominant	c	g	rs13170533	-0.09	0.02	5.5e-06	13034	-0.07	0.02	0.0001	12603	0.6036
Muscle-Dominant	a	c	rs80345488	0.12	0.03	3.4e-06	13034	0.08	0.02	0.002	12603	0.2866
Muscle-Dominant	t	g	rs1028883	-0.04	0.01	0.0009	13034	-0.06	0.01	5.2e-07	12603	0.2087
Muscle-Dominant	a	c	rs6058093	0.04	0.01	9e-05	13034	0.05	0.01	6.1e-07	12603	0.4186
Muscle-Dominant	t	c	rs9306468	0.06	0.01	1.2e-07	13034	0.03	0.01	0.002	12603	0.1136
Peripheral Fat	a	g	rs11205797	-0.05	0.01	6.1e-05	13034	-0.06	0.01	1.1e-05	12603	0.7454
Peripheral Fat	c	g	rs566596164	0.11	0.02	3.3e-09	13034	0.07	0.02	0.0001	12603	0.1651
Peripheral Fat	a	g	rs13172689	-0.08	0.02	4.2e-08	13034	-0.05	0.02	0.0006	12603	0.1549
Peripheral Fat	a	g	rs1651274	-0.06	0.01	6.3e-05	13034	-0.06	0.01	0.0001	12603	0.9333
Peripheral Fat	c	g	rs141783576	-0.13	0.02	3.8e-08	13034	-0.1	0.02	1.8e-05	12603	0.4209
Peripheral Fat	t	c	rs10827616	0.05	0.01	4.4e-05	13034	0.06	0.01	5.2e-06	12603	0.6991
Peripheral Fat	a	g	rs7129492	-0.06	0.01	2.1e-06	13034	-0.06	0.01	1.9e-07	12603	0.6974
Peripheral Fat	t	c	rs11045236	-0.07	0.01	4.5e-06	13034	-0.06	0.02	0.0001	12603	0.6078
Peripheral Fat	a	g	rs11057413	-0.05	0.01	9.7e-05	13034	-0.06	0.01	6.6e-06	12603	0.6319
Peripheral Fat	t	c	rs749170	-0.06	0.01	7.8e-07	13034	-0.05	0.01	8.2e-05	12603	0.512
Peripheral Fat	t	g	rs3116602	-0.08	0.01	1.3e-08	13034	-0.06	0.01	4.6e-05	12603	0.282
Peripheral Fat	a	c	rs9565581	-0.07	0.01	3.7e-09	13034	-0.06	0.01	8.8e-06	12603	0.3337
Peripheral Fat	c	g	rs1883711	-0.12	0.03	0.0009	13034	-0.18	0.04	1.6e-07	12603	0.1588
Peripheral Fat	t	c	rs11698277	-0.07	0.01	1.2e-08	13034	-0.06	0.01	7.9e-07	12603	0.6353
Peripheral Fat	t	c	rs2267373	-0.05	0.01	9.6e-05	13034	-0.07	0.01	1.2e-09	12603	0.1106
Lower Body Fat	t	c	rs12138803	-0.06	0.01	1.4e-05	13034	-0.05	0.01	0.0004	12603	0.5824
Lower Body Fat	c	g	rs55893113	0.05	0.01	7.8e-05	13034	0.06	0.01	2.5e-05	12603	0.8152
Lower Body Fat	a	g	rs754243	0.07	0.01	8.6e-07	13034	0.06	0.01	0.0001	12603	0.4544
Lower Body Fat	t	g	rs1128249	0.08	0.01	2.3e-12	13034	0.06	0.01	3.5e-07	12603	0.1986
Lower Body Fat	t	c	rs2943653	-0.05	0.01	2.7e-05	13034	-0.06	0.01	9.7e-06	12603	0.8323
Lower Body Fat	a	g	rs6822892	-0.04	0.01	0.0021	13034	-0.06	0.01	1.2e-06	12603	0.1887
Lower Body Fat	t	g	rs6888037	-0.06	0.01	3.7e-05	13034	-0.05	0.01	0.0001	12603	0.8521
Lower Body Fat	a	c	rs998584	-0.09	0.01	9.1e-15	13034	-0.06	0.01	4.1e-06	12603	0.03135
Lower Body Fat	a	g	rs72959041	-0.14	0.03	2e-07	13034	-0.11	0.03	4.8e-05	12603	0.4536
Lower Body Fat	a	g	rs7133378	0.08	0.01	3.8e-10	13034	0.04	0.01	0.001	12603	0.03769
Lower Body Fat	t	c	rs3818717	-0.05	0.01	4.4e-05	13034	-0.05	0.01	7.3e-05	12603	0.9724
Lower Body Fat	t	c	rs58542926	-0.15	0.02	3.9e-12	13034	-0.13	0.02	1.1e-08	12603	0.4256
Lower Body Fat	c	g	rs10406327	0.04	0.01	0.001	13034	0.06	0.01	4.8e-07	12603	0.1827
Lower Body Fat	a	g	rs2287922	-0.06	0.01	1.3e-06	13034	-0.04	0.01	0.002	12603	0.2262
Lower Body Fat	a	g	rs3747207	-0.14	0.01	2.5e-23	13034	-0.09	0.01	7.1e-10	12603	0.009817

Supplementary Table 7: Top 10 significant gene sets for General Obesity Axis. Including their effect sizes (Beta), standardised effect sizes (Beta STD), standard errors (SE), and p-values (both unadjusted and Bonferroni-adjusted).

Gene Set	N Genes	Beta	Beta STD	SE	P	Pbon
GOBP_CORTICOSTEROID_RECEPTOR_SIGNALING_PATHWAY	14	0.70491	0.019218	0.18574	7.40E-05	1
GOBP_EMBRYONIC_DIGESTIVE_TRACT_DEVELOPMENT	31	0.60347	0.024471	0.15978	7.96E-05	1
REACTOME_STAT3_NUCLEAR_EVENTS_DOWNSTREAM_OF_ALK_SIGNALING	9	1.0911	0.023853	0.29966	1.36E-04	1
GOBP_TRANSFORMING_GROWTH_FACTOR_BETA2_PRODUCTION	9	1.0485	0.022921	0.29613	2.00E-04	1
WP_THERMOGENESIS	105	0.28806	0.021455	0.082149	2.28E-04	1
WP_MICRORNAS_IN_CARDIOMYOCYTE_HYPERTROPHY	79	0.31485	0.020355	0.090763	2.62E-04	1
GOBP_APPENDAGE_MORPHOGENESIS	142	0.25625	0.022173	0.074035	2.70E-04	1
GERY_CEBP_TARGETS	121	0.26664	0.02131	0.077103	2.72E-04	1
REN_ALVEOLAR_RHABDOMYOSARCOMA_UP	95	0.29985	0.021249	0.086861	2.79E-04	1
BIOCARTA_ALK_PATHWAY	34	0.52742	0.022396	0.15329	2.91E-04	1

Supplementary Table 8. **Top 10 significant gene sets for Muscle-Dominant axis.** Including their effect sizes (Beta), standardised effect sizes (Beta STD), standard errors (SE), and p-values (both unadjusted and Bonferroni-adjusted).

Gene Set	N	Beta	Beta STD	SE	P	Pbon
GOBP_REGULATION_OF_POTASSIUM_ION_IMPORT	4	1.7339	0.025275	0.47811	0.00014398	1
GOBP_CARDIAC_MUSCLE_CELL_ACTION_POTENTIAL_INVOLVED_IN_CONTRAC	47	0.50114	0.025011	0.14055	0.00018194	1
GOMF_ALPHA_ACTININ_BINDING	27	0.64735	0.024501	0.1816	0.00018266	1
GOBP_POTASSIUM_ION_IMPORT_ACROSS_PLASMA_MEMBRANE	45	0.46799	0.022856	0.13189	0.00019435	1
GOBP_DETECTION_OF_MUSCLE_STRETCH	7	1.3578	0.026179	0.38282	0.00019557	1
GOCC_ENDOPLASMIC_RETICULUM_CHAPERONE_COMPLEX	11	0.85939	0.02077	0.24257	0.00019847	1
GOBP_VENTRICULAR_CARDIAC_MUSCLE_CELL_ACTION_POTENTIAL	32	0.61788	0.025455	0.17472	0.00020336	1
PID_ECADHERIN_NASCENT_AJ_PATHWAY	39	0.46398	0.021098	0.13617	0.0003288	1
SCHLINGEMANN_SKIN_CARCINOGENESIS_TPA_DN	24	0.54425	0.019422	0.16346	0.00043573	1

Supplementary Table 9. **Top 10 significant gene sets for Peripheral Fat axis.** Including their effect sizes (Beta), standardised effect sizes (Beta STD), standard errors (SE), and p-values (both unadjusted and Bonferroni-adjusted).

Gene Set	N Genes	Beta	Beta STD	SE	P	Pbon
WHITE_NEUROBLASTOMA_WITH_1P36.3_DELETION	19	1.2182	0.038685	0.29636	1.98E-05	0.33
BILANGES_SERUM_SENSITIVE_VIA_TSC2	28	0.61387	0.023659	0.15615	4.24E-05	0.72
GOCC_PROTEIN_COMPLEX_INVOLVED_IN_CELL_MATRIX_ADHESION	17	0.79412	0.023855	0.20804	6.77E-05	1
GOBP_DIGESTIVE_TRACT_MORPHOGENESIS	48	0.49899	0.025166	0.13326	9.07E-05	1
NOUSHMEHR_GBM_GERMLINE_MUTATED	7	1.0902	0.02102	0.29839	0.00012972	1
WU_APOPTOSIS_BY_CDKN1A_NOT_VIA_TP53	10	0.9723	0.022405	0.29131	0.00042334	1
REACTOME_SUMOYLATION_OF_DNA_METHYLATION_PROTEINS	15	0.77101	0.021757	0.2333	0.00047614	1
GOMF_WNT_RECEPTOR_ACTIVITY	17	0.69733	0.020948	0.21331	0.00054047	1
GOBP_LACRIMAL_GLAND_DEVELOPMENT	7	1.0708	0.020647	0.3321	0.00063236	1
DASU_IL6_SIGNALING_SCAR_DN	15	0.82531	0.023289	0.25799	0.00069078	1

Supplementary Table 10. **Top 10 significant gene sets for Lower Body Fat axis.** Including their effect sizes (Beta), standardised effect sizes (Beta STD), standard errors (SE), and p-values (both unadjusted and Bonferroni-adjusted).

Gene Set	N Genes	Beta	Beta STD	SE	P	Pbon
LINDGREN_BLADDER_CANCER_HIGH_RECURRENCE	47	0.51822	0.025863	0.13544	6.53E-05	1
CAFFAREL_RESPONSE_TO_THC_UP	30	0.55358	0.022083	0.14648	7.89E-05	1
GOBP_REGULATION_OF_ADIPONECTIN_SECRETION	7	1.1143	0.021485	0.2981	9.30E-05	1
GOBP_FOREBRAIN_MORPHOGENESIS	13	0.83411	0.021914	0.22966	0.00014108	1
GOBP_DIACYLGLYCEROL_BIOSYNTHETIC_PROCESS	9	1.1038	0.024132	0.30611	0.00015593	1
GOCC_MRNA_EDITING_COMPLEX	14	0.78114	0.021296	0.21696	0.0001593	1
GAUSSMANN_MLL_AF4_FUSION_TARGETS_C_UP	162	0.23231	0.021459	0.06575	0.00020583	1
GOBP_GLAND_MORPHOGENESIS	120	0.29291	0.023313	0.083554	0.00022838	1
REACTOME_ACYL_CHAIN_REMODELING_OF_DAG_AND_TAG	5	1.2181	0.01985	0.35423	0.00029307	1
GOBP_CARDIAC_ATRIUM_DEVELOPMENT	35	0.54983	0.023688	0.16009	0.00029756	1

Supplementary Table 11: Mendelian Randomization sensitivity analyses for obesity axes. This table presents the sensitivity analyses for the associations between obesity axes and disease outcomes. For each significant association based on the primary IVW method, the table reports the IVW results, and the corresponding results from sensitivity tests. Note that for the General Obesity Axis, which was instrumented with only two SNPs, sensitivity tests were not performed, and only IVW estimates are presented. All p-values are adjusted as described in the Methods.

Outcome	Exposure	Method	Beta	Se	P-value	Upper CI	Lower CI
Asthma	General Obesity Axis	Inverse variance weighted	0.39	0.09	2.80E-05	0.57	0.21
Cholelithiasis	General Obesity Axis	Inverse variance weighted	0.72	0.29	1.38E-02	1.29	0.15
Hip osteoarthritis	General Obesity Axis	Inverse variance weighted	0.85	0.38	2.58E-02	1.60	0.10
Knee osteoarthritis	General Obesity Axis	Inverse variance weighted	0.72	0.36	4.81E-02	1.44	0.01
Chronic kidney disease	Muscle-Dominant Axis	Inverse variance weighted	0.29	0.10	3.58E-03	0.49	0.10
Chronic kidney disease	Muscle-Dominant Axis	MR Egger	1.32	2.59	6.12E-01	6.39	-3.76
Chronic kidney disease	Muscle-Dominant Axis	Simple mode	0.28	0.20	1.57E-01	0.67	-0.11
Chronic kidney disease	Muscle-Dominant Axis	Weighted median	0.26	0.12	3.01E-02	0.49	0.02
Chronic kidney disease	Muscle-Dominant Axis	Weighted mode	0.24	0.16	1.30E-01	0.54	-0.07
Hip osteoarthritis	Muscle-Dominant Axis	Inverse variance weighted	0.33	0.09	3.93E-04	0.51	0.15
Hip osteoarthritis	Muscle-Dominant Axis	MR Egger	-0.75	2.36	7.50E-01	3.88	-5.38
Hip osteoarthritis	Muscle-Dominant Axis	Simple mode	0.25	0.15	8.71E-02	0.55	-0.04
Hip osteoarthritis	Muscle-Dominant Axis	Weighted median	0.22	0.11	4.10E-02	0.44	0.01
Hip osteoarthritis	Muscle-Dominant Axis	Weighted mode	0.25	0.14	8.01E-02	0.53	-0.03
Chronic kidney disease	Peripheral Fat Axis	Inverse variance weighted	-0.17	0.06	6.24E-03	-0.05	-0.30
Chronic kidney disease	Peripheral Fat Axis	MR Egger	-0.60	0.68	3.74E-01	0.73	-1.93
Chronic kidney disease	Peripheral Fat Axis	Simple mode	0.03	0.14	8.59E-01	0.30	-0.25

Chronic kidney disease	Peripheral Fat Axis	Weighted median	-0.15	0.08	6.63E-02	0.01	-0.32
Chronic kidney disease	Peripheral Fat Axis	Weighted mode	-0.14	0.14	3.02E-01	0.13	-0.41
MASLD	Peripheral Fat Axis	Inverse variance weighted	0.28	0.11	1.38E-02	0.50	0.06
MASLD	Peripheral Fat Axis	MR Egger	-0.18	1.21	8.82E-01	2.19	-2.55
MASLD	Peripheral Fat Axis	Simple mode	0.51	0.26	4.77E-02	1.02	0.01
MASLD	Peripheral Fat Axis	Weighted median	0.33	0.15	2.92E-02	0.62	0.03
MASLD	Peripheral Fat Axis	Weighted mode	0.41	0.23	6.75E-02	0.86	-0.03
Polycystic ovary syndrome	Peripheral Fat Axis	Inverse variance weighted	0.40	0.19	3.26E-02	0.77	0.03
Polycystic ovary syndrome	Peripheral Fat Axis	MR Egger	-2.79	2.01	1.66E-01	1.16	-6.74
Polycystic ovary syndrome	Peripheral Fat Axis	Simple mode	0.92	0.40	2.25E-02	1.71	0.13
Polycystic ovary syndrome	Peripheral Fat Axis	Weighted median	0.64	0.22	3.73E-03	1.06	0.21
Polycystic ovary syndrome	Peripheral Fat Axis	Weighted mode	0.58	0.36	1.09E-01	1.30	-0.13
Aortic aneurysm	Lower Body Fat Axis	Inverse variance weighted	-0.36	0.14	8.58E-03	-0.09	-0.62
Aortic aneurysm	Lower Body Fat Axis	MR Egger	0.21	0.58	7.23E-01	1.35	-0.93
Aortic aneurysm	Lower Body Fat Axis	Simple mode	-0.59	0.34	8.31E-02	0.08	-1.26
Aortic aneurysm	Lower Body Fat Axis	Weighted median	-0.14	0.16	3.86E-01	0.17	-0.44
Aortic aneurysm	Lower Body Fat Axis	Weighted mode	-0.12	0.26	6.56E-01	0.39	-0.63
Coronary heart disease	Lower Body Fat Axis	Inverse variance weighted	-0.26	0.12	2.93E-02	-0.03	-0.49
Coronary heart disease	Lower Body Fat Axis	MR Egger	0.54	0.50	2.79E-01	1.51	-0.43
Coronary heart disease	Lower Body Fat Axis	Simple mode	-0.48	0.18	7.25E-03	-0.13	-0.83
Coronary heart disease	Lower Body Fat Axis	Weighted median	-0.31	0.10	1.75E-03	-0.12	-0.51
Coronary heart disease	Lower Body Fat Axis	Weighted mode	-0.49	0.18	5.81E-03	-0.14	-0.84
Hypertension	Lower Body Fat Axis	Inverse variance weighted	-0.08	0.02	3.51E-07	-0.05	-0.11
Hypertension	Lower Body Fat Axis	MR Egger	-0.01	0.07	9.01E-01	0.13	-0.15
Hypertension	Lower Body Fat Axis	Simple mode	-0.11	0.02	3.05E-10	-0.07	-0.14
Hypertension	Lower Body Fat Axis	Weighted median	-0.09	0.01	4.12E-16	-0.07	-0.11
Hypertension	Lower Body Fat Axis	Weighted mode	-0.10	0.02	1.87E-06	-0.06	-0.14
Knee osteoarthritis	Lower Body Fat Axis	Inverse variance weighted	0.20	0.06	2.05E-03	0.32	0.07
Knee osteoarthritis	Lower Body Fat Axis	MR Egger	0.10	0.28	7.20E-01	0.66	-0.45
Knee osteoarthritis	Lower Body Fat Axis	Simple mode	0.18	0.12	1.16E-01	0.41	-0.04
Knee osteoarthritis	Lower Body Fat Axis	Weighted median	0.11	0.06	7.58E-02	0.24	-0.01
Knee osteoarthritis	Lower Body Fat Axis	Weighted mode	0.05	0.08	4.99E-01	0.20	-0.10
MASLD	Lower Body Fat Axis	Inverse variance weighted	-1.58	0.35	6.74E-06	-0.89	-2.26
MASLD	Lower Body Fat Axis	MR Egger	-6.29	1.24	4.42E-07	-3.85	-8.72
MASLD	Lower Body Fat Axis	Simple mode	-0.60	0.17	3.90E-04	-0.27	-0.93
MASLD	Lower Body Fat Axis	Weighted median	-0.63	0.15	1.37E-05	-0.35	-0.92
MASLD	Lower Body Fat Axis	Weighted mode	-0.61	0.16	1.50E-04	-0.29	-0.92
Myocardial infarction	Lower Body Fat Axis	Inverse variance weighted	-0.31	0.11	6.30E-03	-0.09	-0.53
Myocardial infarction	Lower Body Fat Axis	MR Egger	1.04	0.44	1.75E-02	1.91	0.18

Myocardial infarction	Lower Body Fat Axis	Simple mode	-0.44	0.13	9.61E-04	-0.18	-0.71
Myocardial infarction	Lower Body Fat Axis	Weighted median	-0.34	0.08	2.36E-05	-0.18	-0.50
Myocardial infarction	Lower Body Fat Axis	Weighted mode	-0.33	0.11	2.78E-03	-0.11	-0.54
Polycystic ovary syndrome	Lower Body Fat Axis	Inverse variance weighted	-0.39	0.14	3.51E-03	-0.13	-0.66
Polycystic ovary syndrome	Lower Body Fat Axis	MR Egger	0.67	0.58	2.54E-01	1.81	-0.48
Polycystic ovary syndrome	Lower Body Fat Axis	Simple mode	-0.38	0.31	2.22E-01	0.23	-0.99
Polycystic ovary syndrome	Lower Body Fat Axis	Weighted median	-0.36	0.19	6.03E-02	0.02	-0.73
Polycystic ovary syndrome	Lower Body Fat Axis	Weighted mode	-0.30	0.26	2.45E-01	0.20	-0.80
Psoriasis	Lower Body Fat Axis	Inverse variance weighted	-0.33	0.11	3.13E-03	-0.11	-0.55
Psoriasis	Lower Body Fat Axis	MR Egger	-0.72	0.48	1.33E-01	0.22	-1.66
Psoriasis	Lower Body Fat Axis	Simple mode	-0.17	0.19	3.65E-01	0.20	-0.53
Psoriasis	Lower Body Fat Axis	Weighted median	-0.23	0.11	3.72E-02	-0.01	-0.44
Psoriasis	Lower Body Fat Axis	Weighted mode	-0.16	0.16	3.27E-01	0.16	-0.48
Type 2 Diabetes	Lower Body Fat Axis	Inverse variance weighted	-0.72	0.12	6.96E-10	-0.49	-0.95
Type 2 Diabetes	Lower Body Fat Axis	MR Egger	-0.91	0.52	7.89E-02	0.10	-1.92
Type 2 Diabetes	Lower Body Fat Axis	Simple mode	-0.92	0.12	9.59E-14	-0.68	-1.16
Type 2 Diabetes	Lower Body Fat Axis	Weighted median	-0.51	0.06	2.67E-15	-0.39	-0.64
Type 2 Diabetes	Lower Body Fat Axis	Weighted mode	-0.59	0.07	6.32E-16	-0.45	-0.73

A. Male

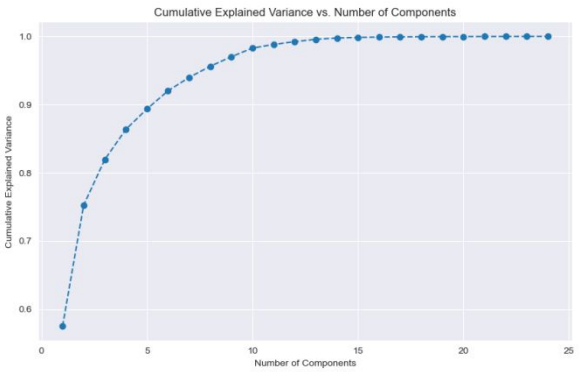

B. Female

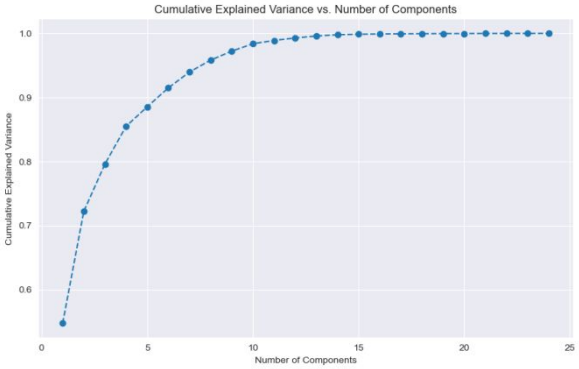

Supplementary Figure 1. Cumulative explained variance versus the number of principal components (PCs) derived from the MRI dataset for (A) males and (B) females. Each plot shows the proportion of variance explained by the PCs cumulatively, highlighting the significant contribution of the first four PCs in capturing the primary patterns of fat and muscle distribution. The elbow point in both graphs indicates diminishing returns in variance explained beyond these components.

A. Male

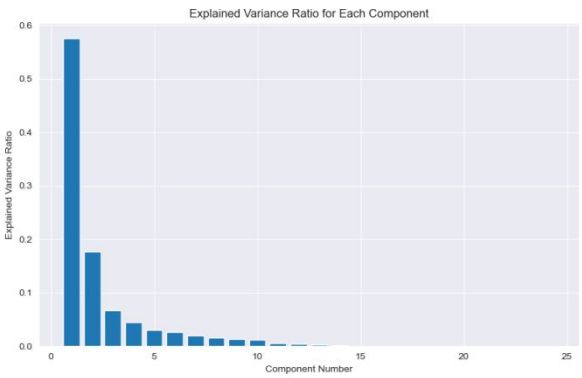

B. Female

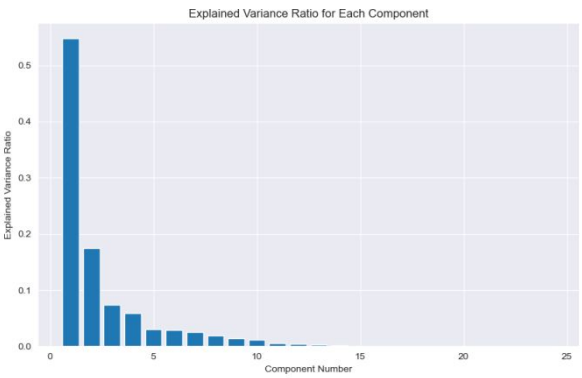

Supplementary Figure 2. Explained variance ratio for each principal component (PC) in the male and female datasets. The bar plots show the proportion of variance explained by each individual PC, demonstrating the significant contributions of the first four PCs in both sexes. These components capture the primary dimensions of variation in fat and muscle distribution derived from the MRI dataset.

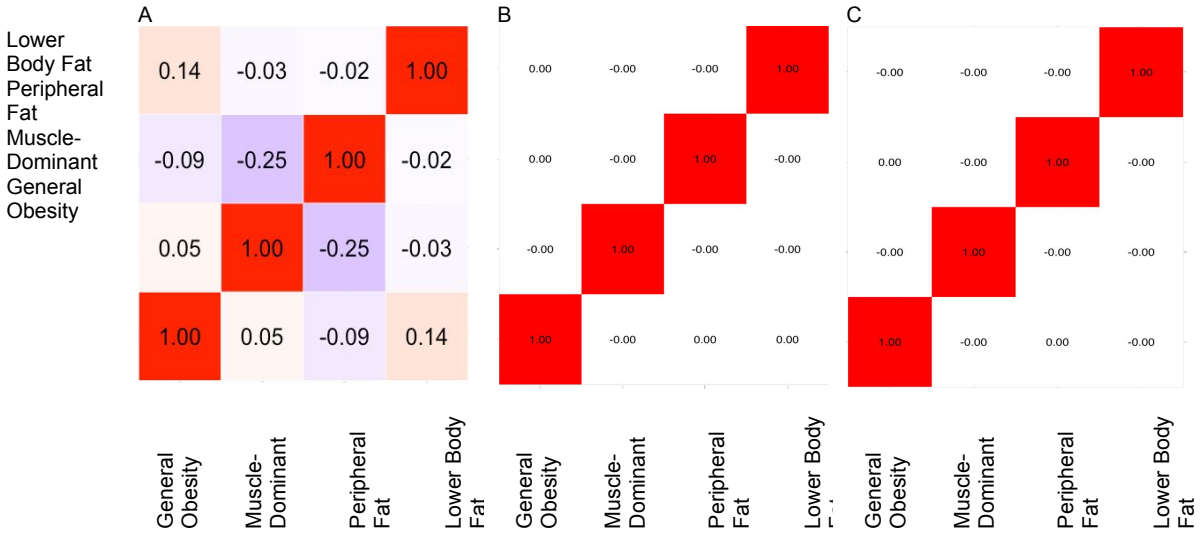

Supplementary Figure 3: The correlation among obesity axes. (A) Genetic correlations among the obesity axes. (B) Phenotypic correlations among the obesity axes in males. (C) Phenotypic correlations among the obesity axes in females. The colors and their intensities represent the genetic correlation coefficients (rg) or the phenotypic correlation coefficients, providing a visual representation of the relationships between different obesity axes.

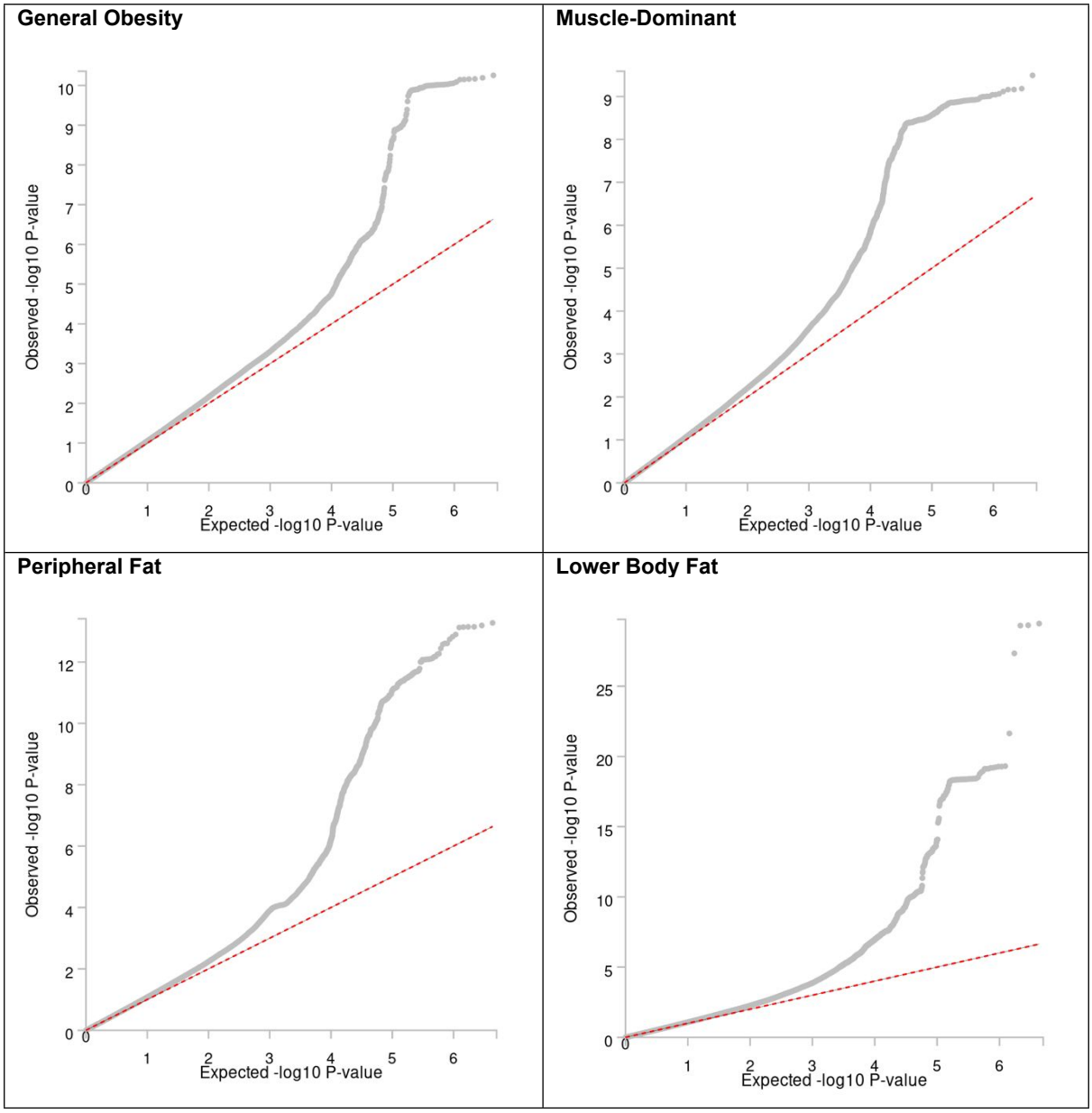

Supplementary Figure 4: QQ plots of the four obesity axes.

General Obesity

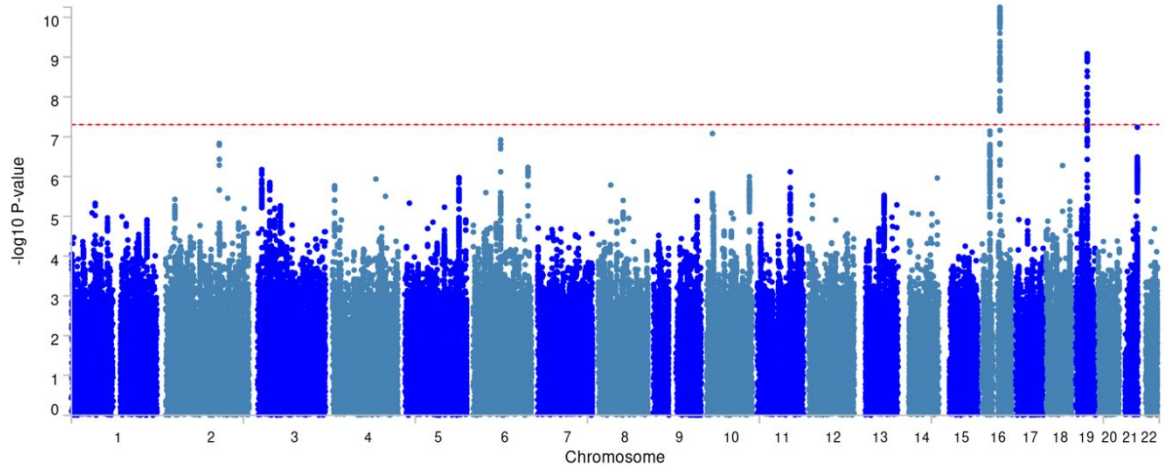

Muscle-Dominant

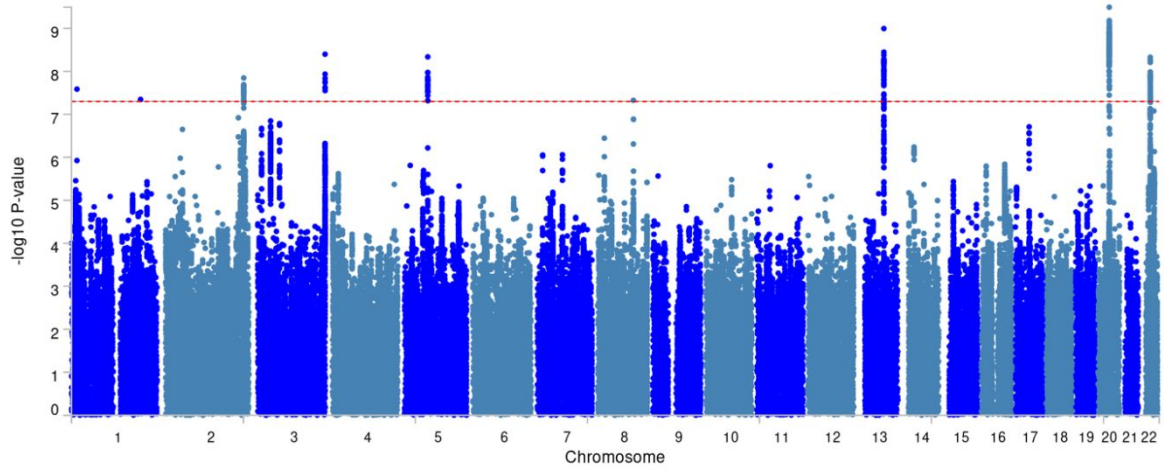

Peripheral Fat

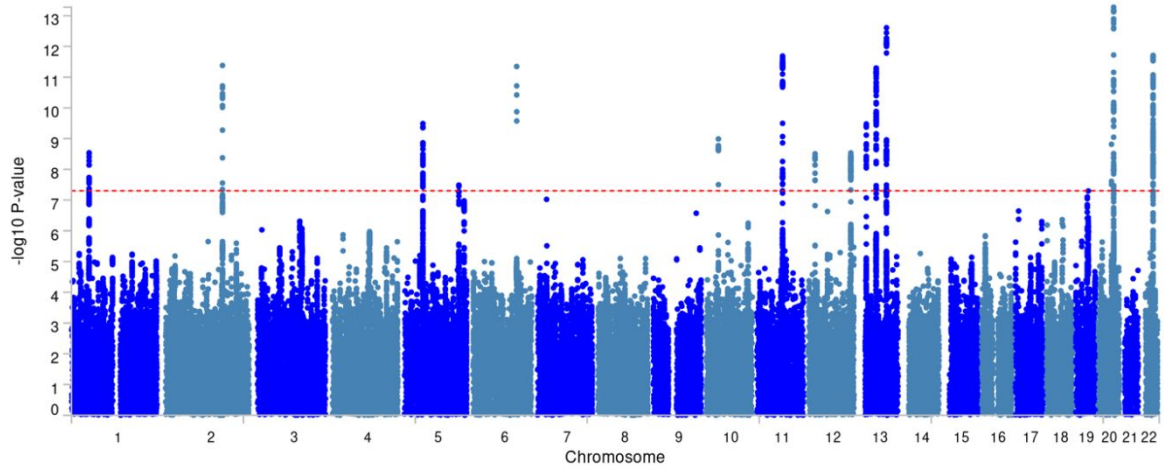

Lower Body Fat

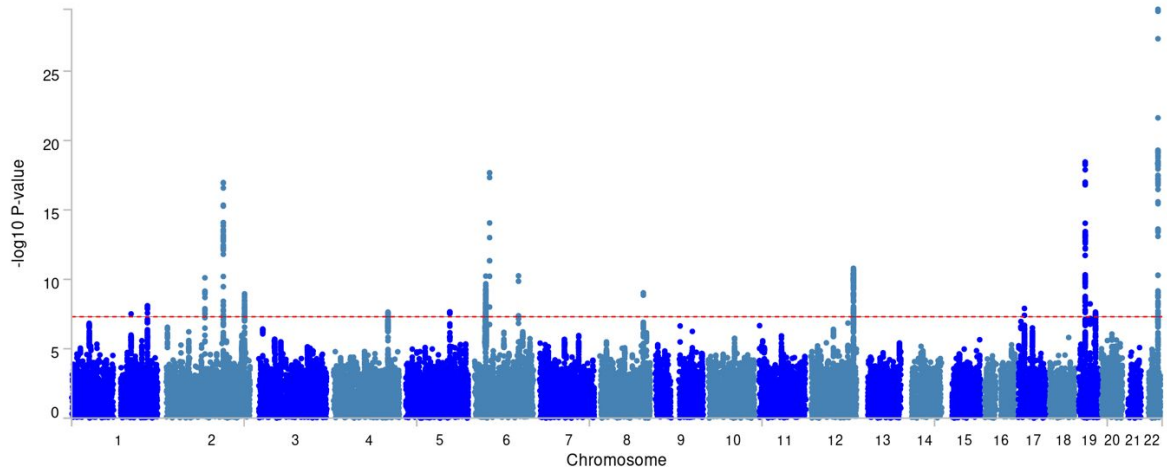

Supplementary Figure 5: Manhattan plots of the four obesity axes.

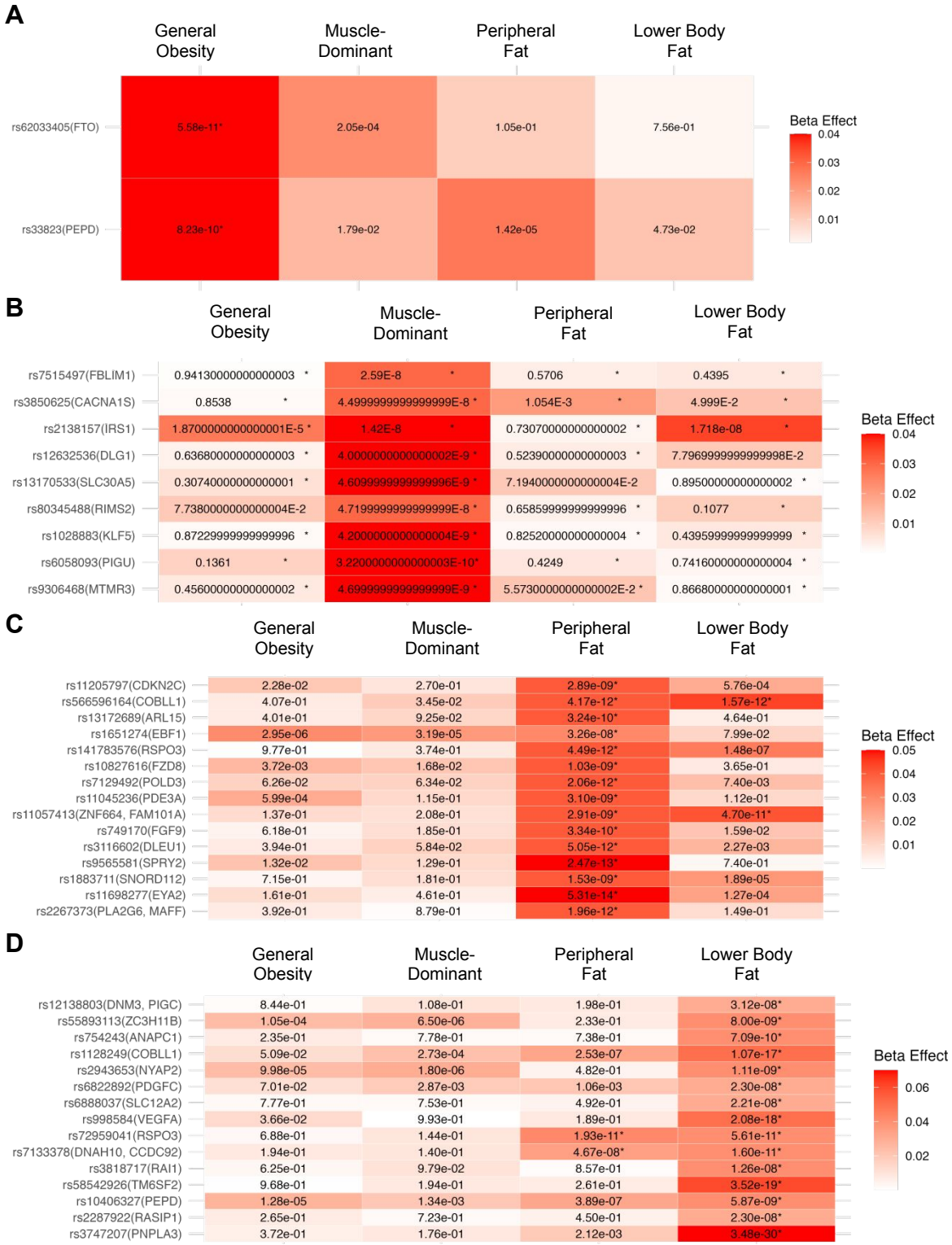

Supplementary Figure 6. The effect of genetic loci associated with (a) General Obesity, (b) Muscle-Dominant, (c) Peripheral Fat, and (d) Lower Body Fat axes on other obesity axes. The color and intensity represent the direction and magnitude of the effect from linear regression in the genome-wide association model, with asterisks indicating associations with a p-value < 5e-08.

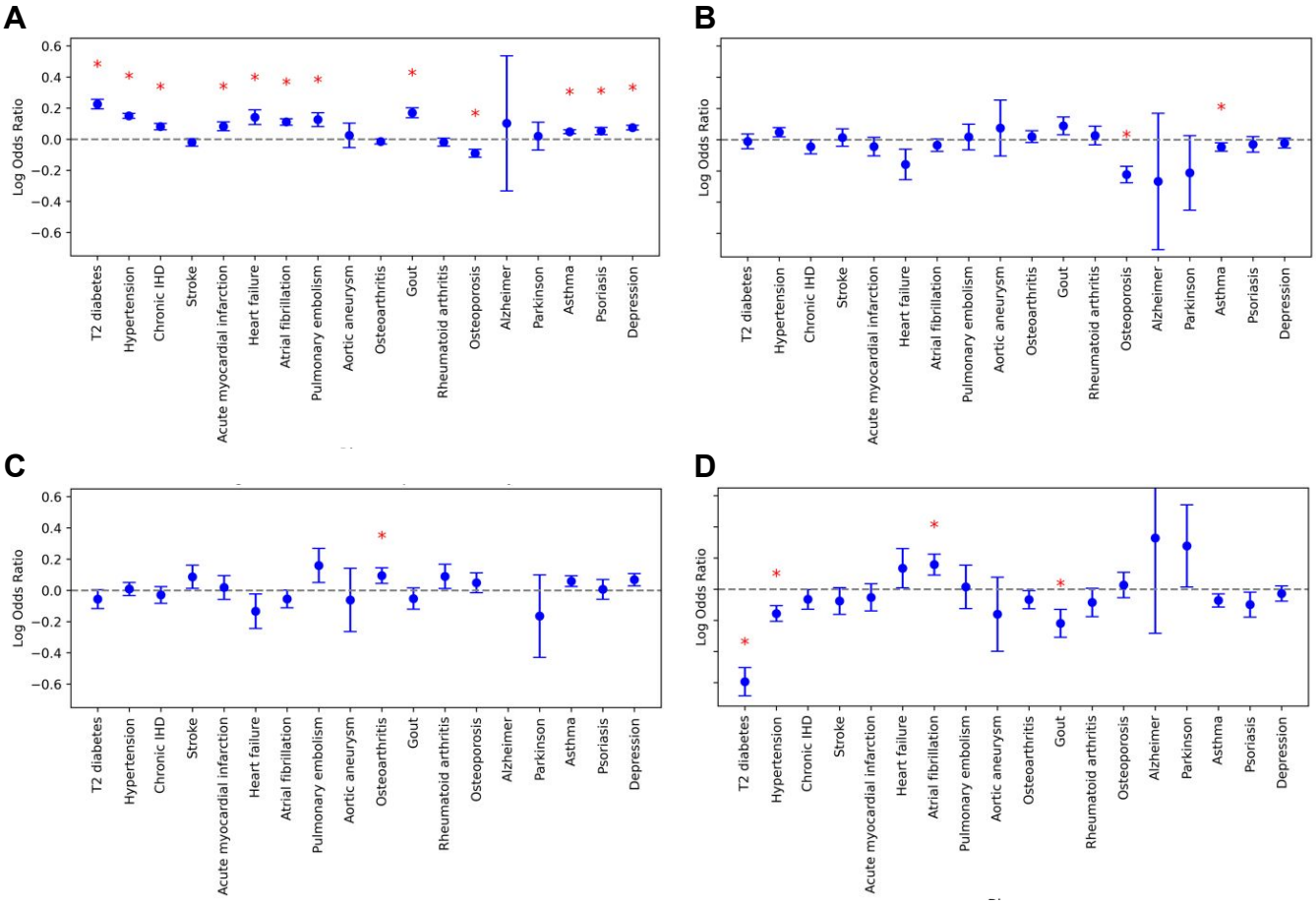

Supplementary Figure 7: Disease risk comparison between top and bottom 10% of each obesity axis. This figure displays the log(odds ratios) for various disease outcomes among individuals in the top 10% compared to those in the bottom 10% for each obesity axis, based on prevalent disease cases. Each pane represents a different axis: (A) General Obesity Axis; (B) Muscle-Dominant Axis; (C) Peripheral Fat Axis; (D) Lower Body Fat Axis. The bars indicate the odds ratios with 95% confidence intervals, illustrating the increased or decreased risk of diseases across these axes. Asterisks denote statistically significant associations after Bonferroni correction ($p < 0.05/18*4$).